Targeting IRE1 with Small Molecules Counteracts Progression of Atherosclerosis

Authors: Ozlem Tufanli[a,b], Pelin Telkoparan Akillilar[a,b,f], Diego Acosta-Alvear[c,,g] Begum Kocaturk[a,b], Ismail Cimen[a,b,h], Umut I. Onat[a,b], Syed M. Hamid[a,b], Peter Walter[c], Christian Weber[d,e], Ebru Erbay[a,b,l]

Affiliations:

[a] Department of Molecular Biology and Genetics, Bilkent University, Ankara, 06800, Turkey

[b] National Nanotechnology Center, Bilkent University, Ankara, 06800, Turkey

[c] Howard Hughes Medical Institute and Department of Biochemistry and Biophysics, University of California at San Francisco, San Francisco, CA 94143, USA

[d] Institute for Cardiovascular Prevention, Ludwig Maximilians University Munich, Munich, 80336, Germany

[e] German Centre for Cardiovascular Research, partner site Munich Heart Alliance, Munich, 80336, Germany

[f] present address: Department of Medical Biology, Yuksek Ihtisas University, Ankara, 06520, Turkey

[g] present address: Department of Molecular, Cellular and Developmental Biology, University of California at Santa Barbara, Santa Barbara, CA 93106, USA

[h] present address: Institute for Cardiovascular Prevention, Ludwig Maximilians University Munich, Munich, 80336, Germany

[1]To whom correspondence should be addressed: eerbay@bilkent.edu.tr

Short Title: IRE1 Inhibitors for Treating Atherosclerosis

CLASSIFICATION: Cell Biology, Medical Sciences

ABSTRACT

Metaflammation, an atypical form of metabolically induced, chronic and low-grade inflammation, plays an important role in the development of obesity, diabetes and atherosclerosis. An important primer for metaflammation is the persistent metabolic overloading of the endoplasmic reticulum, leading to its functional impairment. Activation of the unfolded protein response (UPR), a homeostatic regulatory network that responds to endoplasmic reticulum (ER) stress, is a hallmark of all stages of atherosclerotic plaque formation. The most conserved ER-resident UPR regulator, Inositol-requiring enzyme-1 (IRE1), is activated in lipid-laden macrophages that infiltrate the atherosclerotic lesions. Using RNA sequencing in macrophages, we discovered that IRE1 regulates the expression of many pro-atherogenic genes, including several important cytokines and chemokines. We show that IRE1 inhibitors uncouple lipid-induced ER stress from inflammasome activation in both mouse and human macrophages. *In vivo*, these IRE1 inhibitors led to a significant decrease in IL-1β and IL-18 production that is induced by hyperlipidemia, lowered T helper type-1 immune responses and reduced atherosclerotic plaque size without altering the plasma lipid profiles in the Apolipoprotein E-deficient mice. These results demonstrate that pharmacologic modulation of IRE1 counteracts metaflammation and alleviates atherosclerosis.

KEY WORDS
Endoplasmic reticulum stress, unfolded protein response, metabolic stress, metaflammation, lipotoxicity, atherosclerosis, macrophage

SIGNIFICANCE STATEMENT

ER stress is linked to the development of complex metabolic diseases, including diabetes, obesity and atherosclerosis. Irremediable ER stress can push the UPR towards pro-inflammatory and pro-apoptotic signaling. The need to dissociate the adaptive UPR responses from its destructive outputs has become a major challenge for therapeutic strategies aimed at mitigating ER stress that is often observed in chronic diseases. Our findings show that IRE1 plays a critical role in metaflammation and that administering IRE1-specific inhibitors to hyperlipidemic mice counteracts atherosclerosis progression.

INTRODUCTION

Complex molecular interactions between environment, diet and genetics that take place at the metabolic and immune interface provoke a low-grade, chronic inflammatory response — *metaflammation*— that engages cells of the immune system (macrophages, neutrophils, and lymphocytes) and metabolic tissues (adipocytes, hepatocytes and pancreatic cells) (1). An important primer for metaflammation is chronic metabolic overloading of organelles, such as the endoplasmic reticulum (ER) and mitochondria, which results in impairment of their functions (2).

The ER serves essential cellular functions that include the synthesis and folding of secreted and transmembrane proteins, calcium storage, and lipid synthesis for membrane biogenesis or energy storage (3). Disruption of any of these functions leads to ER stress, and the subsequent activation of an elaborate network of adaptive responses, collectively known as the unfolded protein response (UPR) (3). The UPR re-establishes homeostasis through both transcriptional and translational layers of control (3). The UPR signals through three mechanistically distinct branches that are initiated by the ER-resident protein folding sensors IRE1 (inositol-requiring enzyme 1), PERK (protein kinase RNA-like ER kinase), and ATF6 (activating transcription factor 6) (3).

IRE1 controls the phylogenetically most conserved branch of the UPR, found from fungi to metazoans. It has an ER-lumenal sensor domain that recognizes unfolded peptides, and cytosolic kinase and endoribonuclease (RNase) domains that relay the information to downstream effectors (3). Upon sensing unfolded proteins, IRE1 oligomerizes and *trans*-autophosphorylates, thereby activating its RNase function. Metazoan IRE1 possesses two functional outputs dependent on its RNase activity: i) it initiates a non-conventional splicing reaction that processes XBP1 (X-box binding protein-1)'s mRNA to allow the translation of its active form, XBP1s, a potent transcription factor that, together with ATF6, drives expression of numerous genes, including those encoding ER-resident chaperones and ER-associated protein degradation machinery (3). ii) IRE1 selectively degrades ER-bound mRNAs in a process known as regulated IRE1-dependent decay (RIDD) to alleviate ER load (4). By these mechanisms, UPR activation can reinstate homeostasis.

Increased ER stress and activation of the UPR are well documented in atherosclerosis (5). Many metabolic cardiovascular risk factors observed in obesity, including hyperglycemia, hypercholesterolemia, and elevated saturated fats, can induce ER stress in all stages of atherogenesis, the process leading to the development of atherosclerotic plaques. During atherogenesis, a maladaptive inflammatory response is initiated by the deposition of cholesterol-rich lipoproteins in the sub-endothelial layer of arterial walls (6). Signs of ER stress are most prominent in the atherosclerosis-prone regions of vascular lesions, such as the branching points of arteries, and are typically observed in macrophages among other immune cells infiltrating these regions (7, 8). Chronic, irremediable ER stress triggers apoptosis in macrophages, contributing to the growth of the necrotic core that is observed in atherosclerotic plaques and leads to a subsequent reduction in plaque stability, which promotes their rupture (5) .

Work over the last decade has pinpointed ER stress as a driving force for atherosclerosis progression (5, 7-10). For example, inhibiting the apoptotic signaling downstream of ER stress through genetic deletion of the pro-apoptotic transcription factor CHOP (CCAAT box-binding enhancer homologous protein) or the signal transducer JNK (c-Jun N-terminal kinase) blocks atherosclerosis progression (5, 11-13). Moreover, modulation of ER stress by using chemical chaperones alleviates atherosclerosis, further supporting that therapeutic modulation of ER function is a promising avenue to combat atherosclerosis (14-16). Precedence for this notion is provided by pharmacological approaches to improve ER function — and thereby limit ER stress — that include autophagy inducers, antioxidants, regulators of ER calcium homeostasis and proteostasis (17-19).

Recent drug discovery efforts have opened the door to approaches that entail selective modulation of UPR signaling. This quest has led to the identification of several new small molecules that target the enzymatic activities of specific UPR regulators (19-23). Specifically, blocking IRE1 or XBP1s function has been shown to be beneficial for restraining tumor progression in mouse models (21, 24), highlighting that the specific targeting of the UPR can have beneficial impact in disease models.

Several lines of evidence support the notion that selective pharmacological targeting of IRE1 is a desirable therapeutic approach for treatment of atherosclerosis. First, a profound increase in IRE1 phosphorylation and XBP1s expression is observed in atherosclerotic plaques of mice and humans (8, 10). Second, mechanical sheer stresses activate IRE1, while cardiovascular disease risk factors, such as oxidized phospholipids and homocysteine, can induce both IRE1 and PERK (5, 25-29). Third, experimentally sustained XBP1 mRNA splicing in the vessel wall promotes atherosclerosis, whereas its ablation ameliorated hypercholesterolemia in obese or Apolipoprotein E-deficient ($ApoE^{-/-}$) mice (10, 30). Two small molecules, STF-083010 and 4μ8C, which selectively inhibit IRE1's RNase function, have been used in cells and animals to produce favorable therapeutic outcomes in other disease settings: STF-083010 reduced growth of multiple myeloma (21, 24, 31, 32), and 4μ8c suppressed inflammation in a murine arthritis model (33). The action of both compounds is well understood mechanistically. Both form a Schiff base with a specific lysine positioned in the active site of the IRE1 RNase, blocking its function, and both show no overt toxicity when administered systemically (21, 32, 33). Thus, we reasoned that these drugs may have therapeutic applicability to atherosclerosis.

Here we investigated the direct contribution of IRE1's RNase function to lipid-induced inflammation and to atherosclerotic disease progression by administering these two IRE1 RNase inhibitors to macrophages and to $ApoE^{-/-}$ mice on a Western-type (high fat) diet. Our results substantiate the notion that specific pharmacological modulation of IRE1's RNase activity counteracts metaflammation and yields therapeutic gains in atherosclerotic disease, warranting further validation in human disease.

RESULTS

Pro-atherogenic genes are regulated by IRE1's RNase activity

To understand the contribution of IRE1's RNase activity to atherogenesis, we first analyzed the

impact of its inhibition on the transcriptome of macrophages using RNA-seq. ER poisons, such as tunicamycin, which inhibits protein N-linked glycosylation in the ER lumen, or thapsigargin, which disrupts ER calcium reuptake, activate all UPR branches simultaneously, impeding the dissection of the signaling contributions of individual UPR branches. By refraining from using these pleiotropic drugs, we aimed to identify the specific IRE1 RNase-regulated gene expression changes. To this end, we probed the transcriptional response to acute inhibition of IRE1's RNase activity using STF-083010 in primary mouse bone marrow-derived macrophages (BMDMs). We analyzed differentially regulated mRNAs at early time points (6 hours) after IRE1 inhibition to distinguish immediate-responsive genes from those whose expression may be altered as part of an adaptive response to chronic inhibition. Using an arbitrary cut-off of 1.5-fold, we observed increased expression of 169 genes and decreased expression of 135 genes upon IRE1 RNase inhibition (Fig. 1A, S.Table 1 and S.Table 2; $p<0.05$). To categorize the affected genes functionally according to their association with disease processes, we employed the Ingenuity Pathway Analysis (IPA) tool (34). IPA identified the down-regulation of many important pro-atherogenic genes, including cytokines, chemokines, and chemokine receptors upon inhibition of the steady-state IRE1 activity (Fig. 1B).

We next validated our findings using quantitative reverse transcription polymerase chain reaction (qRT-PCR). In these experiments, we observed a significant reduction in the mRNA levels of IL-1β (interleukin-1β), CCL2 (C-C Motif Chemokine Ligand 2), S100A8 (calgranulin A) and MMP9 (matrix metalloprotease-9) ($p<0.05$, $p<0.001$, $p<0.01$, $p<0.01$, respectively), following IRE1 inhibition either with STF-083010 or 4μ8c (Fig. 1C-E, S.Fig. 1A-E). Consistent with earlier reports, these IRE1 RNase inhibitors had no effect on the kinase function of IRE1 (S.Fig.1F-1H), confirming that the identified pro-atherogetic genes are regulated by IRE1's RNase activity..

Since IRE1 is rate-limiting for the production of XBP1s, we next assessed if XBP1s regulates the expression of these pro-atherogenic genes. To this end, we forced expression of XBP1s or restored IRE1 function in IRE1-deficient ($IRE1^{-/-}$) mouse embryonic fibroblasts (MEF) (S.Fig.1I). Both experiments showed a marked induction of IL-1β, CCL2, and S100A8 mRNA levels (Fig. 1F-H). Together, our findings confirm that the IRE1-XBP1 signaling branch of the UPR maintains the expression of key pro-atherogenic cytokines and chemokines in macrophages.

Induction of IL-1β and CCL2 depends on IRE1 during lipotoxicity

Our finding that IRE1 maintains the expression of several important, pro-atherogenic genes in macrophages suggests that, when induced by metabolic stress, heightened IRE1 activity could drive the atherosclerotic process. One important activating signal for the UPR in macrophages is exposure to excessive amounts of lipids, which elicits toxicity (14, 28, 35). This lipotoxicity results in increased production of reactive oxygen species (ROS), ER stress, and inflammation, and can result in apoptosis (35).

Based on these observations, we next investigated if lipid-induced IRE1 activation plays a role in IL-1β induction. Inhibition of IRE1 with STF-083010 led to a significant block in lipid-induced IL-1β mRNA production and secretion from BMDMs (Fig. 2A-B, S.Fig.2A-B). As expected, inhibition of IRE1 activity with 4μ8c showed the same effects (S.Fig. 2C-F). To further delineate

the role of IRE1 and XBP1s in the regulation of IL-1β, we transfected BMDMs with a specific small interfering RNAs (siRNAs). We found that expression of siRNAs against *IRE1α* (the ubiquitiously expressed IRE1 homolog) or against *XBP1* resulted in a significant reduction in lipid-induced IL-1β mRNA production and IL-1β secretion in BMDMs (Fig. 2C-D; $p<0.05$, $p<0.05$, $p<0.001$, $p<0.001$, respectively and S.Fig. 2G-H). Moreover, treatment of human peripheral blood monocytes (PBMC) with lipids induced IL-1β secretion, which was blocked by pre-incubation with 4μ8c (Fig. 2E-F, S.Fig. 2I). These findings show that IRE1-XBP1 signaling plays an important role in IL-1β mRNA up-regulation and secretion from both mouse and human macrophages.

We also investigated if the pro-atherogenic chemokine, CCL2, is regulated by IRE1 under lipotoxic ER stress conditions. Both STF-083010 and 4μ8c treatment of BMDMs resulted in complete inhibition of lipid-induced CCL2 mRNA production and secretion (S.Fig. 3A-C). Consistent with this observation, siRNAs against *IRE1α* or *XBP1* also suppressed lipid-induced CCL2 production and secretion in BMDMs (S.Fig. 3D-E). Moreover, 4μ8c blocked lipid-induced CCL2 production in human PBMCs (S.Fig. 3F). Collectively, these data show that IRE1 is important for the inflammatory response to lipids and for the production of pro-atherogenic cytokines in both mouse and human macrophages.

Inflammasome activation depends on IRE1 during lipotoxicity

Because IRE1 inhibition leads to a strong suppression of IL-1 β secretion, we reasoned that IRE1 may contribute to the lipid-induced activation of NLRP3 (Nod-like receptor family, pyrin domain containing protein-3) inflammasome, a multicomponent platform that contains caspase-1, and induce the caspase-1-dependent secretion of the pro-inflammatory cytokines IL-1β and IL-18 (36, 37). Previous studies showed that ER stress induces inflammasome activation through several mechanisms including calcium mobilization and the release of reactive oxygen species (mtROS) from damaged mitochondria (38). Because earlier studies from our and other laboratories showed that treatment of macrophages with saturated fatty acids activate IRE1, and because these lipids specifically activated the NLRP3 inflammasome through inducing mtROS production, we sought to investigate this connection further (36, 37, 39). To this end, we first measured mtROS production in cells exposed to lipotoxic stress in the presence of IRE1 inhibitors. We observed that lipid-induced ER stress in BMDMs resulted in dramatically elevated mtROS production, which was completely blocked by 4μ8c treatment (Fig. 3A and S.Fig 4A).

The impact of IRE1 signaling on inflammasome activation has been postulated to be mediated by the IRE1-dependent accumulation of the thioredoxin-interacting protein (TXNIP), an inhibitor of thioredoxin and whose increased levels promote activation of the NLRP3 inflammasome (40). In stark contrast to these earlier findings, which used cells treated with canonical ER poisons, lipid-induced ER stress led to a profound suppression of TXNIP in macrophages that was partially blocked by inhibiting IRE1 (Fig.3B). Moreover, lipid-induced ER stress also induced pro-caspase-1 maturation (indicated by the appearance of the p10 fragment), an effect that was reduced by treatment with IRE1 RNase inhibitors or siRNA-mediated silencing of IRE1α and XBP1 (Fig. 3C, S.Fig.4B-C). Taken together these results indicate that IRE1 plays a crucial role in perpetuating mtROS production and inflammasome activation in cells experiencing lipotoxic ER stress, but that this effect is independent of TXNIP induction. These results demonstrate that

IRE1 plays a major role in controlling IL-1β production through both transcriptional induction of its immature form and promotion of its maturation via the activation of the NLRP3 inflammasome.

Pharmacological inhibition of IRE1 combats atherosclerosis

The evidence presented above suggests that inhibiting IRE1 may impair the progression of atherosclerosis (14, 17, 41). Therefore, we postulated that administration of IRE1 modulators might have beneficial effects by limiting the inflammatory signaling associated with elevated ER stress in a mouse model of atheroslerosis. To test this notion, we challenged $ApoE^{-/-}$ mice with a Western-type (high-fat) diet (12 weeks) and then treated them daily with STF-083010 by intraperitoneal injection (6 weeks) (Fig. 4A). We observed a significant reduction on XBP1s mRNA ($p<0.05$) and modest increases in canonical RIDD target mRNAs ($p<0.05$) in the spleens of treated mice (S.Fig.5 A-C). We detected no differences in body weights, blood glucose levels, and cholesterol profiles between the STF-083010-treated and control groups (S.Table 3; S.Fig. 6). However, the analysis of *en face* aorta preparations showed that chronic administration of STF-083010 led to a significant decrease (35.8%; $p<0.001$) in atherosclerotic lesions when compared to the control group (Fig. 4B). Furthermore, when we evaluated the impact of STF-0803010 on plaque development in the aortic root, we observed a significant reduction (21.4%, $p<0.001$) in the foam cell area (visualized by Oil Red O staining) in the inhibitor-treated group when compared to control mice (Fig. 4C).

Analogous experiments in $ApoE^{-/-}$ mice on Western diet (12 weeks) and exposed to intraperitoneal injections of 4μ8c (4 weeks) produced similar results (Figs. 4D-F). Like in STF-083010-treated mice, 4μ8c treatment led to a significant reduction (45.2%; $p<0.001$) in atherosclerotic lesion area in *en face* aorta preparations (Fig.4E), a significant reduction in XBP1s mRNA in their spleen cells (S.Fig. 7; $p<0.05$), a reduced foam cell area (Fig. 4F), while no overt differences were noted in body weight or blood glucose levels between the inhibitor treated and control mice (S.Table 4). These *in vivo* findings demonstrate that pharmacological inhibition of IRE1 can effectively mitigate plaque development in mice.

Pharmacological inhibition of IRE1 alters plaque composition

Endothelial cells (EC), vascular smooth muscle cells (VSMC), and immune cells such as lymphocytes, dendritic cells, neutrophils and macrophages play important roles in the development of atherosclerotic plaques in the arterial wall. The UPR is activated in many of these cell types and at all stages of atherosclerotic plaque development. This increase in ER stress is also associated with plaque progression, vulnerability to rupture, and acute coronary syndrome in humans (7). Given that IRE1 inhibitors alleviate atherosclerosis in $ApoE^{-/-}$ mice, we next analyzed the impact of these inhibitors on the cellular composition of the lesions. STF-083010 treatment led to a significant reduction (35%; $p<0.01$) in macrophages (as visualized by MOMA-2 staining) infiltrating the aortic root plaques (Fig. 5A). This reduction in macrophage numbers was not the product of increased apoptosis as determined by TUNEL assays in macrophage-enriched areas of the plaques (Fig. 5B). During plaque formation, VSMCs migrate from adventitia to intima, secreting collagen and sealing the fibrous cap of the plaque. The analysis of the lesions in STF-083010-treated mice (with Mason's Trichrome staining) showed there is a significant increase in collagen content that is responsible for tensile strength and elasticity of the plaques (22%; $p<0.05$) without changes in the numbers of the VSMCs

infiltrating the lesions (S.Fig. 8A-B). Finally, STF-083010 treatment did not alter CD3+ T cell numbers in the lesions (S.Fig. 8C). Taken together, these results indicate that the major consequences of IRE1 inhibition include a reduction in macrophages and an increase in collagen deposition in atherosclerotic lesions, which are characteristic of stable plaques.

Last, we sought *in vivo* evidence for the observed inhibition of IL-1β by IRE1 inhibition in macrophages (Figs. 1 and 2). We observed that STF-083010 treatment reduced the expression of IL-1β in the aortic root lesions stained with a specific antibody against IL-1β (Fig. 5C). Together, these results validate our earlier *in vitro* findings and demonstrate the anti-atherogenic effect of IRE1 inhibitors involves a blockage of inflammation in the lesions.

IRE1 inhibitors suppress hyperlipidemia-induced Th-1 immune responses

Atherosclerosis initiation and progression depend on both innate and adaptive immunity pathways. T cells orchestrate adaptive immunity while macrophages bridge innate and adaptive immune processes that contribute to lesion development. T-helper (Th) cells form the majority of lymphocytes in the atherosclerotic plaques. Th-1 cells are pro-inflammatory, produce high amounts of IFN-γ, and contribute to the progression of atherosclerosis. Two other types of lymphocytes implicated in atherosclerosis progression include Th-2 cells, which produce IL-4, and Th-17 cells, which produce IL-17 (42-44). The inflammasome-induced cytokines IL-18 and IL-1β, play an important role in the polarization of Th-1 and Th-17 responses (45). Since inhibition of IRE1 suppressed inflammasome activation (Fig.3C and S.Fig. 4B-C) and IL-1β production in lipid-challenged macrophages (Fig.2), as well as in lesions and tissues (Fig. 5C, S.Fig. 9A-B), we next assessed the impact of IRE1 inhibition on systemic IL-18 levels and Th cell differentiation in hyperlipidemic mice. $ApoE^{-/-}$ mice (on Western diet) that were treated with STF-083010 displayed a significant decrease in plasma IL-18 levels (Fig.6A; $p<0.05$) and a marked reduction in the secretion of IFN-γ —but not of IL-4 or IL-17— from splenocytes (Fig. 6B; $p<0.001$; Fig. 6C-D, S.Fig. 9C-E). We did not observe changes in the overall T cell counts in atherosclerotic lesions after STF-083010 treatment (S.Fig. 8C), indicating that decreased lymphokine production is intrinsic to intracellular signaling and is not t due to a decline in the infiltrating immune cells that produce them. In conclusion, the reduced inflammasome activity in these mice (as measured by IL-1β and IL-18 levels in Fig.5C and 6A) after STF-083010 treatment correlates with the suppression of the Th-1 inflammatory response that is known to promote atherosclerosis development.

DISCUSSION

Studies in mice and humans suggest that chronic ER stress plays an important role in atherosclerosis progression. Therefore, pharmacological manipulation of the UPR —the network of signaling pathways that respond to ER stress— represents a promising therapeutic approach to manage cardiovascular disease (7, 14, 46). The recent discovery of highly selective UPR modulators provides unique opportunities to investigate the contribution of individual UPR branches to the pathogenesis of this disease. Using small molecules that target IRE1, we showed that modulating IRE1 signaling counteracts atherosclerotic plaque formation in mouse models.

First, IRE1 inhibition altered plaque cellular composition mainly by reducing the numbers of macrophages in the atherosclerotic lesions without altering apoptosis. We infer that this effect is likely to stem from reduction in CCL2, a strong macrophage chemo-attractant, consistent with our observations in macrophages treated with IRE1 RNase inhibitors. Alternatively, IRE1 modulators could impact macrophage clearance from lesions by phagocytosis of dying cells. We saw no changes in the apoptotic cell counts in lesions, arguing against this possibility. Nevertheless, more detailed future studies are required to discriminate between these two possibilities.

Second, IRE1 inhibitor-treated mice displayed an increased collagen content in atherosclerotic lesions, which imparts tensile strength and elasticity to the plaques (47). Because we observed no differences in the number of VSMCs in the lesions, the increased collagen deposition may be related to an augmented collagen folding and secretion, which is consequential to enhanced ER function coupled to reduced cleavage by matrix metalloproteases (MMPs). In fact, early in our study we observed that MMP9 is regulated by IRE1, while another study reported RIDD-dependent collagen degradation during ER stress (48). Both observations lend support to our findings and substantiate our hypotheses.

Third, the results from our RNA-seq analyses in macrophages that were treated with IRE1 inhibitors strongly hinted at IRE1's involvement in the production of several pro-atherogenic cytokines, chemokines, and their receptors including IL-1β, CCL2 and chemokine receptor 2 (CCR2). Indeed, IRE1, through XBP1s, regulates IL-1β and CCL2 mRNA induction in lipid stressed macrophages. Moreover, oxidative stress can activate NF-κB (nuclear factor kappa-light-chain-enhancer of activated B cells) and production of CCL2, resulting in the recruitment of monocytes to a growing plaque (7).

Fourth, cholesterol crystals, saturated fatty acids, and ROS accumulate in plaque areas and provide activation signals for activation the NLRP3 inflammasome and subsequent secretion of IL-1β and IL-18 (38). These cytokines generate Th-1-type immune responses that promote plaque progression and unstable lesions (45). Treatment of macrophages with the IRE1 inhibitors suppressed lipid-induced mtROS production and activation of the NLRP3 inflammasome, and subsequent IL-1β secretion. Our results therefore implicate IRE1 activation in the perpetuation of lipid-induced mitochondrial oxidative stress upstream of NLRP3 inflammasome activation, but our data show that this effect is independent of TXNIP induction (38, 40). Furthermore, we confirmed the inhibitory effect of IRE1 inhibitors on hypercholesterolemia-induced IL-1β and IL-18 production *in vivo*, in plaques and in plasma, respectively. Consistent with these observations, treatment with IRE1 inhibitors led to a marked suppression of hyperlipidemia-induced Th-1 immune responses in these mice. We observed no differences in T cell numbers between the IRE1 inhibitor treatment and control groups.

These collective findings show that prevention of inflammasome-associated cytokine production by IRE1 inhibitors *in vivo* has dramatic effects on counteracting atherosclerotic disease progression. While our findings show a clear impact of IRE1 inhibitor on macrophage inflammatory functions, activation of the UPR also occurs in many other lesion-resident cell types. Our results therefore do not exclude the possibility that the anti-atherogenic effects of the

IRE1 inhibition could also involve other lesion-resident cell types that contribute to atherogenesis.

Fifth, the reduction in plaque inflammation and size occurred independent of a correction of elevated plasma lipid levels of IRE1 inhibitor-treated ApoE$^{-/-}$ mice. This notion contrasts with results of a previous study, bearing a liver-specific deletion of *XBP1*, which displayed a profound reduction in plasma cholesterol and triglyceride levels in mice (49). However, it is important to note that this apparent disparity may exclusively result from feedback activation of IRE1 upon genetic loss of XBP1 (49). Notably, additional siRNA-mediated IRE1 depletion partially reverted the hypolipidemic phenotype in vivo, hinting at a RIDD-dependent function that controls lipid metabolism (30). Since XBP1s promotes the transcriptional upregulation of a lipogenic gene program, these findings could be interpreted to mean that the splicing and RIDD outputs of IRE1 have opposing effects on lipid metabolism (30). Moreover, while most of the direct targets of XBP1 that were identified to participate in the triglyceride and sterol lipogenic programs are also RIDD substrates. IRE1 (through its RIDD modality) seems to be able to reduce basal expression of a large number of lipogenic genes independent of XBP1, hinting at a complex lipogenic regulatory program that depends on the interplay between XBP1 and IRE1 signaling (30, 49). Thus, the observed reduction in plaque size in our study is likely to result from IRE1 inhibitor-mediated anti-inflammatory changes and not the product of changes in lipid metabolism.

While we have seen important gains in mitigating atherosclerosis by pharmacologically targeting IRE1 in our experimental models, it is important to note that the other UPR branches, particularly the PERK-CHOP branch, are also induced as atherosclerosis progresses and appear to be instrumental for macrophage apoptosis (5, 11). Previous studies focusing on the engagement of apoptotic pathways initiated by the UPR (such as those mediated by CHOP and JNK) showed that mice deficient for these apoptotic effectors are protected from atherosclerosis (5, 11, 50). Independent of CHOP or JNK engagement, we found in this study that modulating IRE1 signaling *in vivo* with small molecule IRE1 inhibitors modifies a different branch of UPR signaling that impinges on metaflammation and alters the course of atherosclerosis. These results support the notion that it may be possible to uncouple metabolically induced ER stress from inflammation by calibrating UPR signaling, thereby improving the clinical outcome of atherosclerosis. With the advent of specific inhibitors that can target different UPR branches, exploring the efficacy of combinatorial UPR calibration in this chronic disease setting becomes a promising endeavor.

EXPERIMENTAL PROCEDURES

A list of primers used in the study can be found in the supplemental materials..

Reagents and Plasmids

IRE1$^{-/-}$ MEFs were provided by Gokhan Hotamişligil (Harvard School of Public Health). BMDMs were isolated from of C57BL/6 mice. Plasmids encoding XBP1s (21833), wt IRE1α (13009) were purchased from Addgene. L-Glutamine, Dulbecco's modified Eagle's medium (DMEM), phosphate buffered saline (PBS), Hank's balanced salt solution (HBSS), penicillin/streptomycin (P/S), fetal bovine serum (FBS), and RPMI-1640 medium were obtained

from Thermo Scientific or HyClone (GE Healthcare Life Sciences). Trypsin, ampicillin, kanamycin, Bradford assay reagents, ultrapure lipopolysaccharides (LPS), palmitic acid, phosphatase inhibitor cocktail, and STF-083010 were purchased from Sigma. 4μ8c was purchased from Calbiochem. Primary antibodies used for immunoblotting were purchased from the following suppliers: Anti-IRE1 phospho S724 antibody (Abcam ab48187), IL-1β (Abcam ab9722), IRE1α Rabbit mAb (3294, Cell Signaling), β-Actin (sc-47778, Santa Cruz Biotechnology), β-actin (sc-9104, Santa Cruz Biotechnology), Caspase-1 (M20) (sc-514, Santa Cruz Biotechnology) and IL-1β (R&D Systems_AF-401-NA). Enhanced chemiluminescence Prime Western Blot Detection Kit was purchased from Amersham Pharmacia.

Preparation of PA-bovine serum albumin complex

PA was dissolved in absolute ethanol to yield a stock concentration of 500 mM and stored at −80 °C. Stock PA was diluted to the working concentration and suspended with 1% fatty acid free BSA in RPMI1640 medium (without serum) by mixing at 50°C for 30 minutes.

Cell Culture and Treatments

Isolation of BMDM: Bone marrows were collected from the tibia and femurs of mice into RPMI-1640 medium containing 1% penicillin/streptomycin (P/S). After filtering through a cell strainer (BD Biosciences, 352350), the cells were centrifuged at 400 x g for 5 minutes and resuspended in RPMI-1640 medium enriched with 15% L929 conditioned medium and 1% P/S, followed by seeding for growth and differentiation into macrophages on petri dishes for 7 days.

Inflammasome activation: BMDMs were pre-treated (1 hour) with 100 μM STF-083010 or with the indicated concentrations of 4μ8c, followed by stimulation with ultrapure LPS (200 ng/ml) for 3 hours, then followed by treatment with palmitate-BSA (1000 μM) for 20 hours. Human PBMCs were purchased from Zenbio (Research Triangle Park, NC, USA) and grown in lymphocyte medium (RPMI-1640, 2 mM L-glutamine, 10% fetal bovine serum, and 1% P/S) according to instructions provided by the manufacturer. Cells were pretreated with 100 μM 4μ8c before stimulation with ultrapure LPS (200 ng/ml) for 3 hours. This was followed by treatment with ethanol-BSA (control) or palmitate-BSA (500 μM).

Induction of mtROS: BMDM were pre-treated (1 hour) with 100 μM 4μ8c, followed by sequential stimulation with 200 ng/ml LPS (3 hours) followed by PA/BSA (1000 μM) or vehicle (ethanol)-BSA (control) for 20 hours.

Western blot analysis

Cells were lysed in lysis buffer (50 mM (4-(2-hydroxyethyl)-1-piperazineethanesulfonic acid (HEPES) pH 7.9, 100 mM sodium chloride, 10 mM ethylendiamine tetraacetic acid (EDTA), 10 mM sodium fluoride, 4 mM tetrasodium diphosphate, 1% Triton X-100, 2 mM sodium orthovanadate, 1 mM phenylmethanesulfonyl fluoride (PMSF), 1X phosphatase inhibitor cocktail (Sigma) and 1X protease inhibitor cocktail (Sigma). Lysates were cleared by brief centrifugation followed by the addition of 5X SDS loading dye. For the detection of cleaved caspase-1 (active p10 form) in the cell medium, cell culture supernatants were collected and mixed with 5X SDS loading dye, heated at 95°C for 5 minutes before loading on SDS-PAGE gels. Proteins were subjected to SDS-PAGE separation and transferred onto PVDF membranes. Blocking and antibody incubation were carried out in TBS with 0.1% Tween-20 (v/v) and 5% (w/v) dry milk or BSA and visualized by enhanced chemiluminscence in a BioRad imager.

Transfection
IRE1$^{-/-}$ MEFs that reached 60-80% confluence were transfected with the indicated plasmids (2 μg DNA for every 4.5 x 10^5 cells) with polyethylenimine (Sigma) and BMDMs were electroporated using a Neon electroporator (Invitrogen) according to protocols provided by the manufacturer.

RNA Interference
BMDMs were transfected with 50 nM siRNA against IRE1 (Qiagen; SI0099588), 70 nM siRNA against XBP1 (Qiagen; SI01473227) or scrambled siRNAs (Qiagen; 1027281). 24 hrs after transfection, the cells were treated with indicated reagents.

RNA Isolation and Quantitative RT-PCR
Trisure (Bioline) was used to isolate total RNA from cells and reverse-transcribed using RevertAid First strand cDNA synthesis kit (Thermoscientific; K1691) according to the manufacturer's protocols. cDNAs were amplified using specific primers on a Rotor Gene (Qiagen) real-time PCR instrument. Roche SYBR Green was used for qRT-PCR. Primers are listed in the Supplemental Information. Quantifications were performed using the ΔΔCt method and gene expression levels were normalized to GAPDH or β-actin transcript levels using the following formula: (Primer efficiency)$^{-\Delta\Delta Ct}$ where ΔΔCt means ΔCt (target gene) - ΔCt (reference gene) and Ct means (threshold cycle). We analyzed the results from three or more independent experiments using the Student's t-test.

RNA-seq Library Preparation and Sequencing
Total RNA was isolated from control and IRE1-inhibited (with STF-083010) BMDM samples using Trisure (Bioline). To remove genomic DNA contamination, the RNA samples were treated with 20U of DNase I (New England Biolabs). The RNA concentrations were measured using a NanoDrop ND-2000 Spectrophotometer. Total RNA quality was checked using an Agilent Technologies 2100 Bioanalyzer. Ribosomal RNA was depleted from 5 μg of total RNA using Ribo-Zero Gold rRNA Removal (Epicentre Biotechnologies) following the manufacturer's recommendations. Sequencing libraries for whole transcriptome analysis were prepared using ScriptSeqTM v2 RNA-Seq Library Preparation Kit (Epicentre Biotechnologies) following the manufacturer's recommendations. After 3′-terminal tagging, the di-tagged cDNA was purified using column concentrators (DNA clean-up and concentrators, Zymo Research). The cDNA libraries were bar-coded to allow sample multiplexing using ScriptSeqTM Index PCR Primers (Epicentre Biotechnologies). The libraries were amplified by 12 cycles of PCR and the amplified libraries were size selected and purified using 8% TBE acrylamide gels. The libraries were quantified using Agilent Technologies 2100 Bioanalyzer. Up to four RNA-seq Libraries were then multiplexed in a single lane of an Illumina HiSeq2500 deep-sequencer flow cell (UCSF Center for Advanced Technologies) and sequenced using 50 bp single-end sequencing chemistry.

RNA Sequencing Data Processing
The 3' adapter sequences (AGATCGGAAGAGCACACGTCTGAAC) were removed from the sequenced libraries using the FastQ/A clipper found in the FastX toolkit (http://hannonlab.cshl.edu/fastx_toolkit/) after de-multiplexing, and only reads longer than 20 nucleotides were kept for alignment. The adapter-stripped reads were then aligned the Bowtie indices for the mouse genome reference version 10 of the University of California Santa Cruz

Genome Browser (mm10), using the splice junction mapper Tophat2 v2.0.9 and the sequence aligner Bowtie 2 V2.2.3.0. using default parameters. The transcript assembler Cufflinks V2.1.1 was then used on the list of mapped reads to assemble and quantify transcripts using an mm10 reference annotation and masking mitochondrial, rRNA, and tRNA sequences. To estimate the changes in gene expression levels, the number of sequenced reads that align to a gene of interest was then compared among biological samples using Cuffdiff (default parameters). Changes in the levels of expression of normalized Cufflinks-quantified transcripts are expressed as FPKM/RPKM (reads per kilobase per million reads mapped) values.

Flow Cytometric Analysis of Intracellular Cytokine Staining

Fresh splenocytes were prepared from mice spleen and erythrocytes were removed using red blood cell lysis buffer as described earlier (37). Cells were stimulated for 4h with phorbol-myristate-acetate (PMA) (50 ng/ml, Abcam) and ionomycin (1 μg/ml, Abcam) in the presence of Golgistop (BD Biosciences). Live cells were discriminated from dead ones by using Zombie Green (BioLegend). Cell surfaces were stained with PerCP-Cy5.5-conjugated anti-CD4 antibody (BD Biosciences) followed by incubation in Cytofix/Cytoperm solution (BD Biosciences) at room temperature for 15 min. Then, intracellular cytokines were stained with APC-conjugated IFNγ, PE-conjugated IL-17A and PE-conjugated IL-4 antibodies (all from BD Biosciences). Data were analyzed on BD Accuri C6 software.

Measurement of Secreted IL-1β and IL-18 and CCL2 Cytokines

An IL-1β Elisa Kit (Abcam) was used for detecting IL-1β, mouse IL-18 ELISA Kit (Medical & Biological Laboratories) and a mouse CCL2 Elisa Kit (Abcam) was used for detecting the respective cytokines in mouse plasma or from conditioned medium, as indicated, according to manufacturer's instructions.

Plasma measurements

Fast-performance liquid chromatography (FPLC) was used for analyzing the size distribution of lipoproteins. All measurements were carried out at the Mouse Metabolic Phenotyping Center at the University of Cincinnati. For the resolution of major lipoprotein classes from plasma; the columns were equilibrated in 50 mM phosphate-buffered saline. Using a microtiter plate enzyme-based assay, the major lipoprotein classes were measured in cholesterol or triglyceride assays from collected fractions.

Staining of Cryosections

Cryosections (7 μm thick) were cut from the aortic root of the frozen heart tissue with a cryostat (Leica CM1850) and stained with Oil Red O, anti-MOMA-2 (ab33451; Abcam), anti-CD3-Alexa488 (1:400; Biolegend), TUNEL kit (11684795910; Roche), anti-α-SMA (ab5694; Abcam) and IL-1β antibody (ab9722, Abcam). Imunofluorescent stainings were mounted with an antifade reagent including DAPI (GR211467-2, Abcam). Representative images were taken with a Zeiss fluorescent microscope. Collagen content of the lesions was determined with Masson's trichrome staining as per the manufacturer's protocol (Bio-Optica). Heart tissue sections were stained with Oil Red O stain for plaque area quantifications in accord with previously published protocols (37). All quantifications were performed using ImageJ (National Institutes of Health). Percentage of average cross-sectional stained area per leaflet was calculated from all three valves.

Atherosclerotic Lesion Analysis
Aortas were pinned on a black wax surface and atherosclerotic lesions were analyzed in the aortic arch, and descending aorta by Sudan IV staining as described earlier (37). Areas were quantified using ImageJ and expressed as the percentage of the total aorta area.

Quantification of mtROS
mtROS production was measured with MitoSOX™ Red mitochondrial superoxide indicator (M36008, Life Technologies) according to the protocol provided by the company. Representative images were acquired with a confocal microscope (Zeiss, LSM 510) and analyzed with ImageJ.

Mice and Treatments
$ApoE^{-/-}$ mice in a C57Bl/6 background (Charles River WIGA GmbH, Sulzfeld, Germany) were used in atherosclerosis experiments. Starting from 8 weeks of age, male mice were fed a Western diet (TD88137 mod. containing 21% fat and 0.2% cholesterol) (Ssniff, Soest, Germany) for 6 weeks. Then the mice were injected with STF-083010 (10 mg/kg) or DMSO, both given in 16% Cremophor EL (Sigma) saline solution via intraperitoneal injections, as described previously, for 6 more weeks while mice were continued on the Western diet (21). The other $ApoE^{-/-}$ mice that were used in atherosclerosis experiments were fed a Western diet for 8 weeks. Then they were injected with 4μ8c (10 mg/kg) or DMSO, both given in 16% Cremophor EL saline solution via intraperitoneal injections as described previously (33), for 4 more weeks while mice were continued on Western diet. Weights were measured every other day, while blood glucose concentrations were measured before and after treatments. At the end of the experiment, mice were anaesthetized and blood was collected by cardiac puncture. Bone marrow, spleen and liver tissues were collected and frozen immediately into liquid nitrogen and stored at -80 $^{\circ}$C. Perfusion was performed with ice-cold PBS and heparin (1000 U/ml), followed by 10% formalin solution. After fixation, the aorta was dissected intact, immersed immediately in 10% formalin and stored at 4 $^{\circ}$C until analysis. The heart was removed at the proximal aorta and placed into a tissue mold, covered with OCT (Tissue-Tek), frozen in cold isobutene solution and stored in -80 $^{\circ}$C. All animal experiments were performed according to approved protocols by the experimental animal care committee at Bilkent University.

Statistical Analysis
Values are expressed as mean ± SEM. No samples were treated as outliers and left out of analysis. Statistical significance was evaluated using the Student's *t* test or Mann Whitney test (for *in vivo* analysis, as indicated in the figures). $P<0.05$ were considered as significant.

ACKNOWLEDGMENTS

We express our appreciation to Gokhan S. Hotamisligil (Harvard University) for providing $IRE1^{-/-}$ MEFs, Esther Lutgens and Dirk Lievens for technical advice on bone marrow derived macrophages and Buket Gültekin for administrative help, and Mojtaba Beyramzadeh for technical assistance with atherosclerosis studies. **Funding**: This work was funded in part by the TUBITAK-BMBF Intensified Cooperation grant – 110S293 (to EE and CW) and by an ERC Starting Grant - 336643 (to EE). DAA was supported by an Irvington Postdoctoral Fellowship of the Cancer Research Institute. PW is an Investigator of the Howard Hughes Medical Institute.

REFERENCES:

1. Wellen KE & Hotamisligil GS (2005) Inflammation, stress, and diabetes. *J Clin Invest* 115(5):1111-1119.
2. Hotamisligil GS (2010) Endoplasmic reticulum stress and the inflammatory basis of metabolic disease. *Cell* 140(6):900-917.
3. Walter P & Ron D (2011) The unfolded protein response: from stress pathway to homeostatic regulation. *Science* 334(6059):1081-1086.
4. Hollien J, *et al.* (2009) Regulated Ire1-dependent decay of messenger RNAs in mammalian cells. *J Cell Biol* 186(3):323-331.
5. Zhou AX & Tabas I (2013) The UPR in atherosclerosis. *Seminars in immunopathology* 35(3):321-332.
6. Williams KJ & Tabas I (1995) The response-to-retention hypothesis of early atherogenesis. *Arteriosclerosis, thrombosis, and vascular biology* 15(5):551-561.
7. Tabas I (2010) The role of endoplasmic reticulum stress in the progression of atherosclerosis. *Circ Res* 107(7):839-850.
8. Myoishi M, *et al.* (2007) Increased endoplasmic reticulum stress in atherosclerotic plaques associated with acute coronary syndrome. *Circulation* 116(11):1226-1233.
9. McAlpine CS & Werstuck GH (2013) The development and progression of atherosclerosis: evidence supporting a role for endoplasmic reticulum (ER) stress signaling. *Cardiovascular & hematological disorders drug targets* 13(2):158-164.
10. Zeng L, *et al.* (2009) Sustained activation of XBP1 splicing leads to endothelial apoptosis and atherosclerosis development in response to disturbed flow. *Proceedings of the National Academy of Sciences of the United States of America* 106(20):8326-8331.
11. Thorp E, *et al.* (2009) Reduced apoptosis and plaque necrosis in advanced atherosclerotic lesions of Apoe-/- and Ldlr-/- mice lacking CHOP. *Cell Metab* 9(5):474-481.
12. Ricci R, *et al.* (2004) Requirement of JNK2 for scavenger receptor A-mediated foam cell formation in atherogenesis. *Science* 306(5701):1558-1561.
13. Babaev VR, *et al.* (2016) Jnk1 Deficiency in Hematopoietic Cells Suppresses Macrophage Apoptosis and Increases Atherosclerosis in Low-Density Lipoprotein Receptor Null Mice. *Arteriosclerosis, thrombosis, and vascular biology*.
14. Erbay E, *et al.* (2009) Reducing endoplasmic reticulum stress through a macrophage lipid chaperone alleviates atherosclerosis. *Nat Med* 15(12):1383-1391.
15. Ishimura S, *et al.* (2014) Reduction of endoplasmic reticulum stress inhibits neointima formation after vascular injury. *Sci Rep* 4:6943.
16. Wang B, *et al.* (2014) The modulation of endoplasmic reticulum stress by chemical chaperone upregulates immune negative cytokine IL-35 in apolipoprotein E-deficient mice. *PLoS One* 9(1):e87787.
17. Engin F & Hotamisligil GS (2010) Restoring endoplasmic reticulum function by chemical chaperones: an emerging therapeutic approach for metabolic diseases. *Diabetes Obes Metab* 12 Suppl 2:108-115.
18. Ong DS & Kelly JW (2011) Chemical and/or biological therapeutic strategies to ameliorate protein misfolding diseases. *Curr Opin Cell Biol* 23(2):231-238.
19. Hetz C, Chevet E, & Harding HP (2013) Targeting the unfolded protein response in disease. *Nat Rev Drug Discov* 12(9):703-719.
20. Atkins C, *et al.* (2013) Characterization of a novel PERK kinase inhibitor with antitumor and antiangiogenic activity. *Cancer Res* 73(6):1993-2002.
21. Papandreou I, *et al.* (2011) Identification of an Ire1alpha endonuclease specific inhibitor with cytotoxic activity against human multiple myeloma. *Blood* 117(4):1311-1314.
22. Sidrauski C, *et al.* (2013) Pharmacological brake-release of mRNA translation enhances cognitive memory. *Elife* 2:e00498.

23. Das I, *et al.* (2015) Preventing proteostasis diseases by selective inhibition of a phosphatase regulatory subunit. *Science* 348(6231):239-242.
24. Mimura N, *et al.* (2012) Blockade of XBP1 splicing by inhibition of IRE1alpha is a promising therapeutic option in multiple myeloma. *Blood* 119(24):5772-5781.
25. Gargalovic PS, *et al.* (2006) The unfolded protein response is an important regulator of inflammatory genes in endothelial cells. *Arteriosclerosis, thrombosis, and vascular biology* 26(11):2490-2496.
26. Gora S, *et al.* (2010) Phospholipolyzed LDL induces an inflammatory response in endothelial cells through endoplasmic reticulum stress signaling. *Faseb j* 24(9):3284-3297.
27. Outinen PA, *et al.* (1999) Homocysteine-induced endoplasmic reticulum stress and growth arrest leads to specific changes in gene expression in human vascular endothelial cells. *Blood* 94(3):959-967.
28. Feng B, *et al.* (2003) The endoplasmic reticulum is the site of cholesterol-induced cytotoxicity in macrophages. *Nat Cell Biol* 5(9):781-792.
29. Zhou J, Lhotak S, Hilditch BA, & Austin RC (2005) Activation of the unfolded protein response occurs at all stages of atherosclerotic lesion development in apolipoprotein E-deficient mice. *Circulation* 111(14):1814-1821.
30. So JS, *et al.* (2012) Silencing of Lipid Metabolism Genes through IRE1alpha-Mediated mRNA Decay Lowers Plasma Lipids in Mice. *Cell Metab* 16(4):487-499.
31. Volkmann K, *et al.* (2011) Potent and selective inhibitors of the inositol-requiring enzyme 1 endoribonuclease. *J Biol Chem* 286(14):12743-12755.
32. Cross BC, *et al.* (The molecular basis for selective inhibition of unconventional mRNA splicing by an IRE1-binding small molecule. *Proceedings of the National Academy of Sciences of the United States of America* 109(15):E869-878.
33. Qiu Q, *et al.* (2013) Toll-like receptor-mediated IRE1alpha activation as a therapeutic target for inflammatory arthritis. *Embo j* 32(18):2477-2490.
34. Kramer A, Green J, Pollard J, Jr., & Tugendreich S (2014) Causal analysis approaches in Ingenuity Pathway Analysis. *Bioinformatics (Oxford, England)* 30(4):523-530.
35. Schaffer JE (2003) Lipotoxicity: when tissues overeat. *Curr Opin Lipidol* 14(3):281-287.
36. Wen H, *et al.* (2011) Fatty acid-induced NLRP3-PYCARD inflammasome activation interferes with insulin signaling. *Nature immunology* 12(5):408-415.
37. Çimen I, *et al.* (2016) Prevention of atherosclerosis by bioactive palmitoleate through suppression of organelle stress and inflammasome activation. *Sci Transl Med* 8(358):358ra126.
38. Guo H, Callaway JB, & Ting JP (2015) Inflammasomes: mechanism of action, role in disease, and therapeutics. *Nat Med* 21(7):677-687.
39. Robblee MM, *et al.* (2016) Saturated Fatty Acids Engage an IRE1α-Dependent Pathway to Activate the NLRP3 Inflammasome in Myeloid Cells. *Cell Rep* 14(11):2611-2623.
40. Lerner AG, *et al.* (2012) IRE1alpha induces thioredoxin-interacting protein to activate the NLRP3 inflammasome and promote programmed cell death under irremediable ER stress. *Cell Metab* 16(2):250-264.
41. Kraskiewicz H & FitzGerald U (2011) InterfERing with endoplasmic reticulum stress. *Trends Pharmacol Sci* 33(2):53-63.
42. Zhou X, Paulsson G, Stemme S, & Hansson GK (1998) Hypercholesterolemia is associated with a T helper (Th) 1/Th2 switch of the autoimmune response in atherosclerotic apo E-knockout mice. *J Clin Invest* 101(8):1717-1725.
43. Whitman SC, Ravisankar P, & Daugherty A (2002) IFN-gamma deficiency exerts gender-specific effects on atherogenesis in apolipoprotein E-/- mice. *J Interferon Cytokine Res* 22(6):661-670.
44. Huber SA, Sakkinen P, David C, Newell MK, & Tracy RP (2001) T helper-cell phenotype regulates atherosclerosis in mice under conditions of mild hypercholesterolemia. *Circulation* 103(21):2610-2616.

45. Ait-Oufella H, Taleb S, Mallat Z, & Tedgui A (2011) Recent advances on the role of cytokines in atherosclerosis. *Arteriosclerosis, thrombosis, and vascular biology* 31(5):969-979.
46. Austin RC (2009) The unfolded protein response in health and disease. *Antioxid Redox Signal* 11(9):2279-2287.
47. Adiguzel E, Ahmad PJ, Franco C, & Bendeck MP (2009) Collagens in the progression and complications of atherosclerosis. *Vascular medicine (London, England)* 14(1):73-89.
48. Hollien J & Weissman JS (2006) Decay of endoplasmic reticulum-localized mRNAs during the unfolded protein response. *Science* 313(5783):104-107.
49. Lee AH, Scapa EF, Cohen DE, & Glimcher LH (2008) Regulation of hepatic lipogenesis by the transcription factor XBP1. *Science* 320(5882):1492-1496.
50. Kwok KH*, et al.* (2016) Adipose-Specific Inactivation of JNK Alleviates Atherosclerosis in ApoE-deficient Mice. *Clinical science (London, England : 1979)*.

FIGURE LEGENDS

Figure 1. IRE1 regulates the expression of pro-atherogenic genes. (A) RNA-seq analysis in BMDMs treated with STF-083010 or DMSO (control). Volcano plot of differentially expressed **m**RNAs. **(B)** Analysis of atherosclerosis-related mRNAs using the IPA tool (see text for details). **(C-E)** Confirmation of IRE1-dependent atherogenic gene regulation in mouse BMDMs treated with STF-083010 or DMSO (control) by qRT-PCR. **(F-H)** qRT-PCR analysis of atherogenic gene expression in $IRE1^{-/-}$ MEFs upon forced expression of XBP1s or upon restoring IRE1's function. Data: mean values ± SEM; n = 3; $^{***}p\leq0.001$, $^{**}p\leq0.01$, $^{*}p\leq0.05$, n.s. = not significant; Student's t test).

Figure 2. IRE1 regulates lipid-induced IL-1β secretion in mouse and human macrophages. IL-1β mRNA **(A)** and protein **(B)** levels measured from LPS-primed and PA-stimulated mouse BMDMs treated with STF-083010 or DMSO (control) by qRT-PCR and ELISA, respectively. IL-1β mRNA **(C)** and protein **(D)** levels measured from LPS-primed and PA-stimulated mouse BMDMs transfected with siRNAs against IRE1α or XBP1 and treated with STF-083010 or DMSO (control) by qRT-PCR and ELISA, respectively. **(E)** Secreted IL-1β from LPS-primed, PA-stimulated human PBMCs and treated with or without 4μ8c measured by ELISA. **(F)** Same as E, but protein levels were measured by immunoblotting to show the immature and processed forms of the cytokine (representative image of three independent blots). Statistics as in Fig. 1.

Figure 3. IRE1 inhibitors block lipid-induced mtROS release and inflammasome activation. (A) mtROS production measured in LPS- primed, PA-stimulated mouse BMDM after 4μ8c or DMSO (control) treatment. **(B)** Levels of TXNIP mRNA measured by qRT-PCR in LPS-primed, PA-stimulated mouse BMDM cells treated with 4μ8c or DMSO (control) and **(C)** Immunoblot of the levels of the zymogen (p45) and mature (p10) forms of caspase-1 in LPS-primed, PA-stimulated mouse BMDM cells treated with 4μ8c or DMSO (control). CE: cell extract. SN: supernatant. Statistics as in Fig. 1.

Figure 4. IRE1 inhibitors reduce plaque area in a mouse model of atherosclerosis. (A) Experimental design. **(B)** *En face* aorta analysis of atherosclerotic plaques in $ApoE^{-/-}$ mice. Left: Sudan IV staining of atherosclerotic plaques. Right: quantification of plaque area. (n = 13 to 14).

(**C)** Analysis of aortic sinus plaque area analysis in the animals in A, B. Left: Oil Red O staining of aorta cross sections. Right: quantification of plaque area. (n = 5 to 6). **(D-F)** Experimental design and data for analogous experiments in $ApoE^{-/-}$ mice using a different IRE1 inhibitor (**E,** n = 7 to 9; **F**, n = 5) Scale bar: 350μm. Statistics as in Fig. 1.

Figure 5. IRE1 inhibitors alter plaque composition and inflammation. Immunohistochemical and TUNEL assay analyses of proximal aorta cryosections from $ApoE^{-/-}$ mice treated with an IRE1 inhibitor. In each case a representative image is shown on the left and the quantification of the data appears on the right. **(A)** Monocyte/macrophage marker-2 (MOMA-2). Scale bar: 100μm **(B**) TUNEL assay (apoptotic cells are shown with arrows). Scale bar: 50μm. **(C)** IL-1β. Scale bar: 100μm. Statistics as in Fig. 1.

Figure 6. IRE1 inhibitors suppress hyperlipidemia-induced Th-1 immune responses and IL-18 cytokine levels. (A) Plasma IL-18 in ApoE-/- mice treated with and IRE1 inhibitor measured by ELISA (n = 7). **(B-D)** Flow cytometry analysis of IFNγ, IL-4 and IL-17 in splenocytes from ApoE-/- mice treated with IRE1 inhibitor and activated with PMA/ionomycin (n=5). Statistics as in Fig. 1.

A.

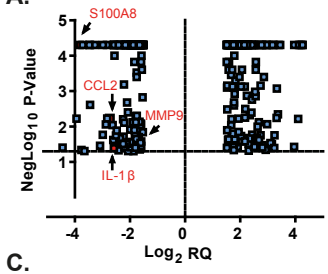

B.

Symbol	Entrez Gene Name	Expression value	
		Fold Change	p-value
S100A8	s100 Calcium Binding Protein A8	-3,83	5,00E-05
CCR2	Chemokine (C-C) Motif Receptor 2	-2,98	5,00E-05
CCL2	The chemokine (C-C motif) ligand 2	-2,73	6,00E-03
IL-1β	Interleukin 1, Beta	-2,58	4,09E-02
CCR3	Chemokine (C-C) Motif Receptor 3	-2,48	1,30E-02
PLA2R1	Phospholipase A2 Receptor 1	-2,04	2,72E-02
ITGA4	Integrin, Alpha 4	-1,93	5,00E-05
MMP9	Matrix Metallopeptidase 9	-1,62	3,91E-02

C.

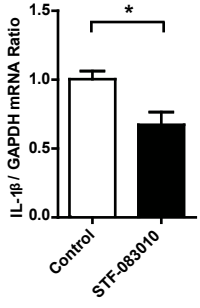

D.

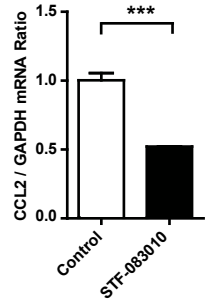

E.

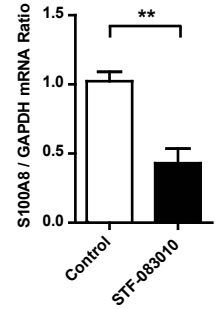

F.

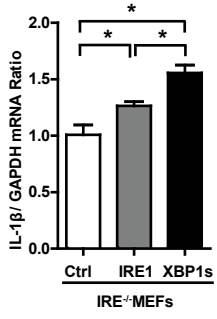

G.

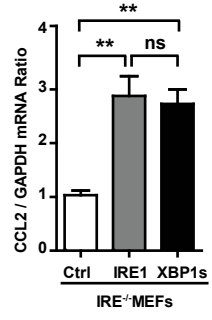

H.

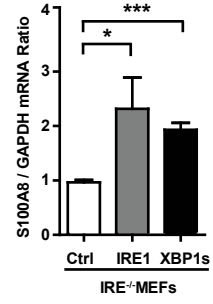

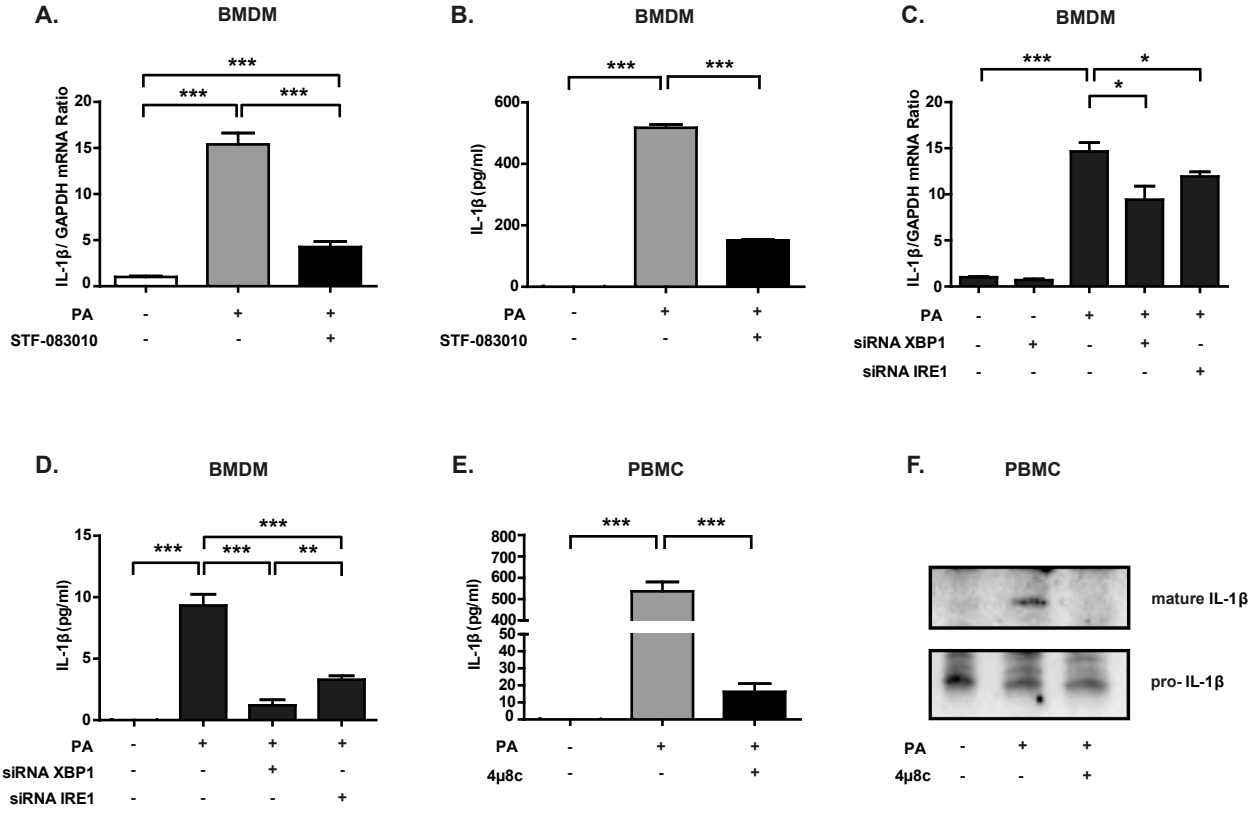
A.
BMDM
IL-1β/ GAPDH mRNA Ratio
PA
STF-083010
B.
BMDM
IL-1β (pg/ml)
PA
STF-083010
C.
BMDM
IL-1β/GAPDH mRNA Ratio
PA
siRNA XBP1
siRNA IRE1
D.
BMDM
IL-1β (pg/ml)
PA
siRNA XBP1
siRNA IRE1
E.
PBMC
IL-1β (pg/ml)
PA
4μ8c
F.
PBMC
mature IL-1β
pro- IL-1β
PA
4μ8c

A.

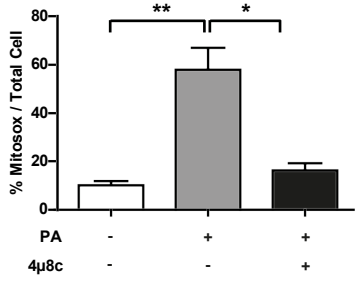
% Mitosox / Total Cell
80
60
40
20
0
**
*
PA - + +
4μ8c - - +

B.

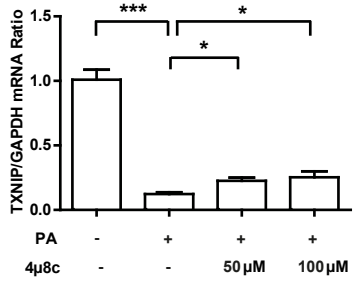
TXNIP/GAPDH mRNA Ratio
1.5
1.0
0.5
0.0
***
*
*
PA - + + +
4μ8c - - 50 μM 100 μM

C.

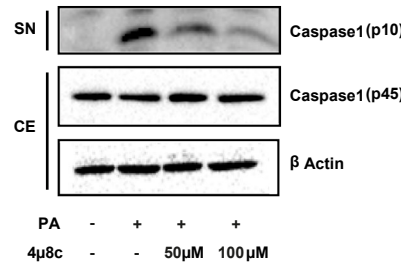
SN
CE
Caspase1(p10)
Caspase1(p45)
β Actin
PA - + + +
4μ8c - - 50μM 100 μM

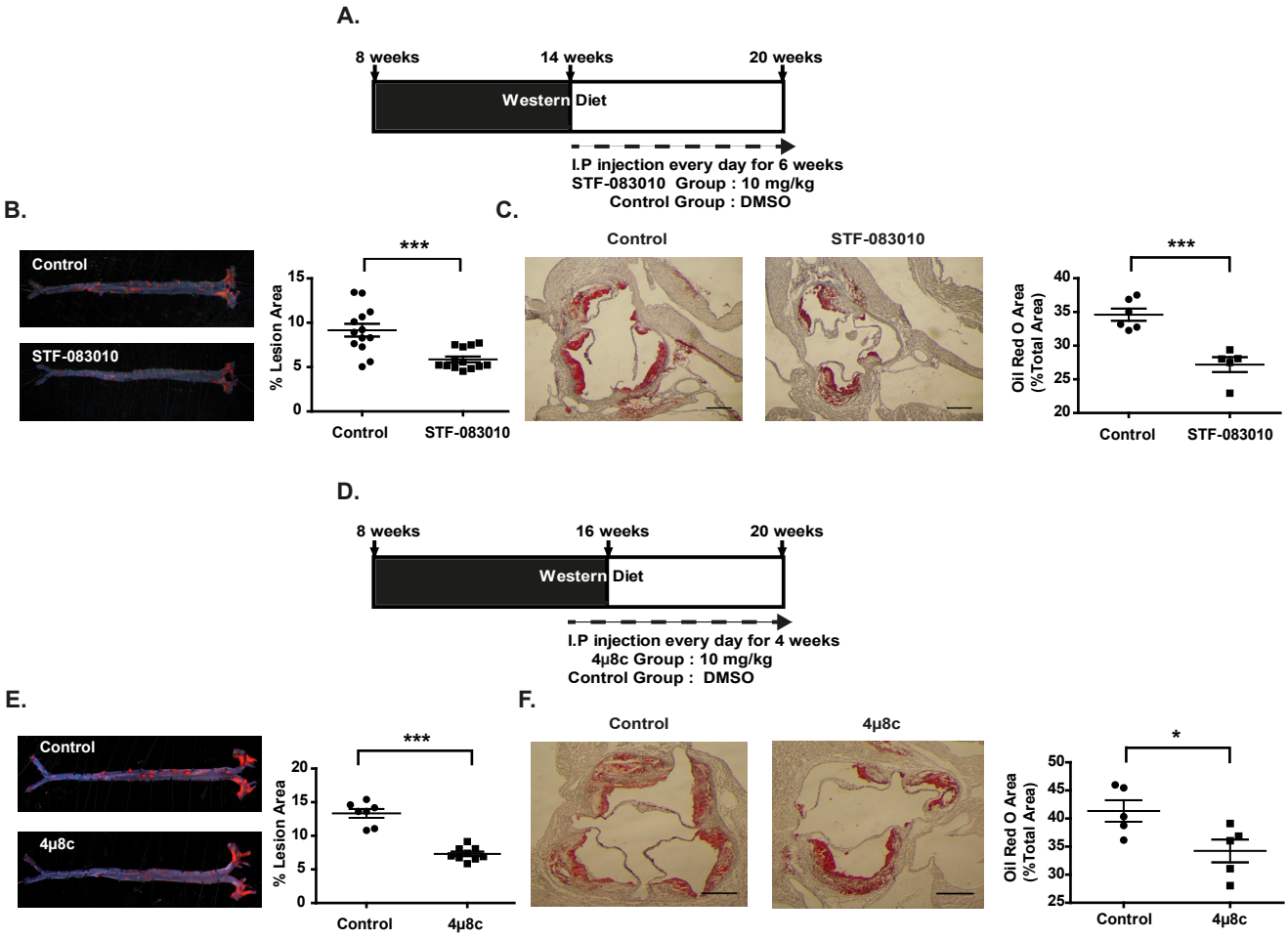
A.
8 weeks
14 weeks
20 weeks
Western Diet
I.P injection every day for 6 weeks
STF-083010 Group : 10 mg/kg
Control Group : DMSO
B.
Control
STF-083010
% Lesion Area
***
Control
STF-083010
C.
Control
STF-083010
Oil Red O Area (%Total Area)
***
Control
STF-083010
D.
8 weeks
16 weeks
20 weeks
Western Diet
I.P injection every day for 4 weeks
4μ8c Group : 10 mg/kg
Control Group : DMSO
E.
Control
4μ8c
% Lesion Area
***
Control
4μ8c
F.
Control
4μ8c
Oil Red O Area (%Total Area)
*
Control
4μ8c

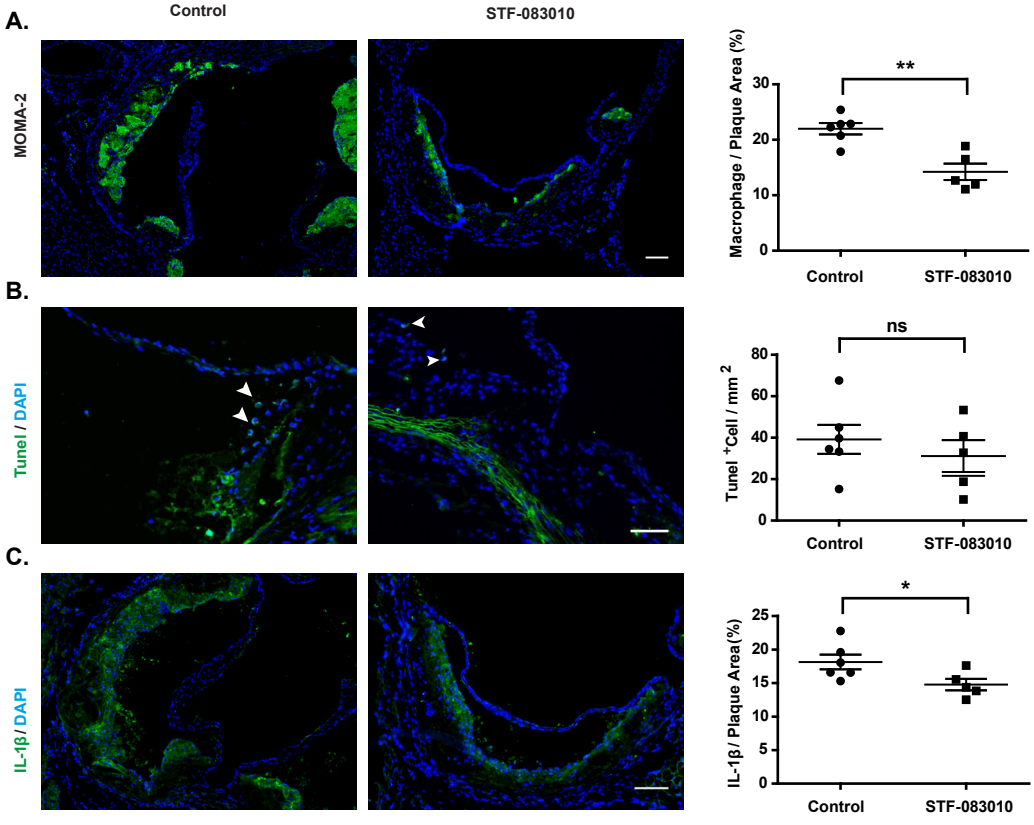
A.
Control
STF-083010
MOMA-2
Macrophage / Plaque Area (%)
**
30
20
10
0
Control
STF-083010
B.
Tunel / DAPI
Tunel +Cell / mm 2
ns
80
60
40
20
0
Control
STF-083010
C.
IL-1β / DAPI
IL-1β / Plaque Area (%)
*
25
20
15
10
5
0
Control
STF-083010

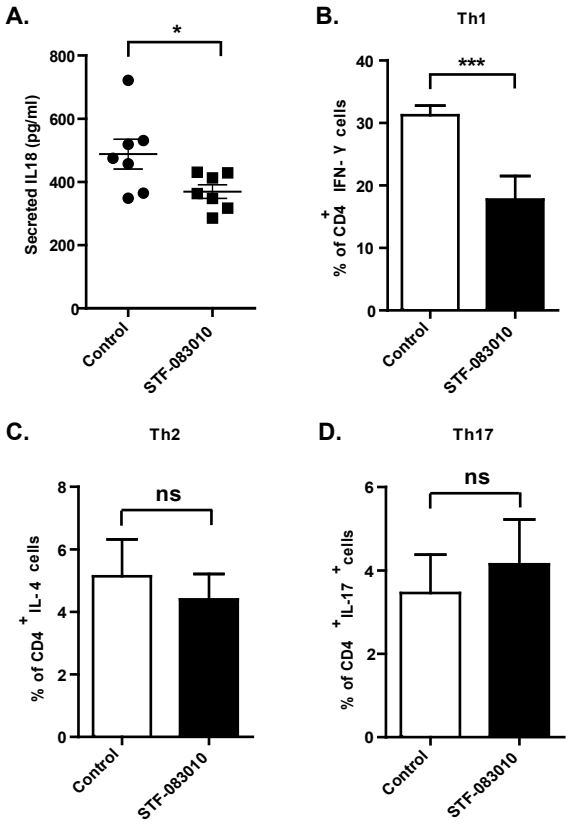
A.
*
800
600
400
200
0
Secreted IL18 (pg/ml)
Control
STF-083010
B.
Th1
***
40
30
20
10
0
% of CD4+ IFN-γ cells
Control
STF-083010
C.
Th2
ns
8
6
4
2
0
% of CD4+ IL-4 cells
Control
STF-083010
D.
Th17
ns
6
4
2
0
% of CD4+ IL-17+ cells
Control
STF-083010

SUPPLEMENTAL INFORMATION

Targeting IRE1 with Small Molecules Counteracts Atherosclerosis

Authors: Ozlem Tufanli[a, b], Pelin Telkoparan[a, b, f], Diego Acosta-Alvear[c, g], Begum Kocaturk[a, b], Ismail Cimen[a, b], Umut I. Onat[a, b], Syed M. Hamid[a, b], Peter Walter[c], Christian Weber[d, e], Ebru Erbay[a, b, 1]

Affiliations:

[a] Department of Molecular Biology and Genetics, Bilkent University, Ankara, 06800, Turkey

[b] National Nanotechnology Center, Bilkent University, Ankara, 06800, Turkey

[c] Department of Biochemistry and Biophysics, University of California at San Francisco, San Francisco, CA, 94143, USA

[d] Institute for Cardiovascular Prevention, Ludwig Maximilians University Munich, Munich, 80336, Germany.

[e] German Centre for Cardiovascular Research, partner site Munich Heart Alliance, Munich, 80336, Germany.

[f] present address: Department of Medical Biology, Yuksek Ihtisas University, Ankara, 06520, Turkey

[g] present address: Department of Molecular, Cellular, and Developmental Biology, University of California at Santa Barbara, Santa Barbara, CA 93106, USA

[1]To whom correspondence should be addressed: eerbay@bilkent.edu.tr

SUPLEMENTAL EXPERIMENTAL PROCEDURES:

Real time PCR primers

Gene	Forward	Reverse
Human		
GAPDH	GACCACAGTCCATGCCATCACT	TCCACCACCCTGTTGCTGTAG
XBP1	TGCTGAGTCCGCAGCAGGTG	GCTGGCAGGCTCTGGGGAAG
CCL2	CTTCTGCGCCTGCTGTTCA	CCAGCCTACTCATTGGGATCA
IL-1β	TTACAGTGGCAATGAGGATGAC	GTCGGAGATTCGTAGCTGGAT
Mouse		
XBP1	TGAGAACCAGGAGTTAAGAACACGC	CCTGCACCTGCTGCGGAC
GAPDH	GTGAAGGTCGGTGTGAACG	GGTCGTTGATGGCAACAATCTC
CCL2	CTTCTGGGCCTGCTGTTCA	CCAGCCTACTCATTGGGATCA
IL-1β	CAACCAACAAGTGATATTCTCCATG	GATCCACACTCTCCAGCTGCA
MMP9	CTGGACAGCCAGACACTAAAG	CTCGCGGCAAGTCTTCAGAG
S100A8	AAATCACCATGCCCTCTACAAG	CCCACTTTTATCACCATCGCAA
β-ACTIN	TTCGTTGCCGGTCCACACCC	GCTTTGCACATGCCGGAGCC
GAPDH	TGAGAACCAGGAGTTAAGAACACGC	CCTGCACCTGCTGCGGAC
PDGFRB	AACCCCCTTACAGCTGTCCT	TAATCCCGTCAGCATCTTCC
SCARA3	TGCATGGATACTGACCCTGA	GCCGTGTTACCAGCTTCTTC

SUPLEMENTARY FIGURE LEGENDS:

Figure S1. Modulation of IRE1 signaling by various methods: validation and impact on various pro-atherogenic genes. **(A)** qRT-PCR analysis of MMP9 mRNA levels in mouse BMDMs treated with STF-083010 or DMSO (control). **(B-E)** qRT-PCR analysis of IL-1β, CCL2, S100A8, and MMP9 mRNA levels in mouse BMDMs treated with 4μ8c or DMSO (control). **(F)** Validation for treatments in Fig.1A-E and S1A: IRE1 phosphorylation was detected by Western blot in lysates of PA-stimulated BMDMs treated with STF-083010 or DMSO (control). **(G-H)** Validation for treatment in Fig. S1B-E: **(G)** qRT-PCR analysis of XBP1s mRNA levels in mouse BMDMs treated with increasing doses of 4μ8C. **(H)** Western blot analysis of IRE1 phosphorylation in BMDMs after IRE1 inhibition with 4μ8c. **(I)** Validation for treatments in Fig. 1F-H: qRT-PCR analysis of XBP1s mRNA levels in IRE1$^{-/-}$ MEFs transfected with plasmids encoding IRE1 or XBP1s. Statistics as in Fig. 1.

Figure S2. Inhibition of IRE1 by various methods in lipid-stressed macrophages: validation and its impact on IL-1β (A-B) Validation of STF-083010 treatments for Figs. 2A-B: **(A)** qRT-PCR analysis of XBP1s mRNA levels in LPS-primed, PA-stimulated mouse BMDMs treated with STF-083010 or DMSO (control) **(B)** Western Blot analysis of p-IRE in LPS-primed, PA-stimulated mouse BMDMs treated with STF-083010 or DMSO (control). **(C-F)** Inhibition of IRE1 RNase activity by 4μ8c and its impact on IL-1β: **(C)** qRT-PCR analysis of IL-1β mRNA levels in LPS-primed, PA-stimulated mouse BMDMs treated with 4μ8c. **(D)** Western Blot analysis of secreted mature IL-1β from LPS-primed, PA-stimulated BMDMs treated with 4μ8c or DMSO (control). **(E)** qRT-PCR analysis of XBP1s mRNA levels in LPS-primed, PA-stimulated mouse BMDMs treated with 4μ8c or DMSO (control). **(F)** Western blot analysis of IRE1 phosphorylation in LPS-primed, PA-stimulated mouse BMDMs treated with 4μ8c or DMSO (control). **(G-H)** Validation of IRE1 and XBP1s knock down in Figs. 2C-D: qRT-PCR analysis of (G) IRE1 or (H) XBP1s mRNA levels in LPS-primed, PA-stimulated mouse BMDMs transfected with siRNAs against IRE1α or XBP1. **(I)** Validation of 4μ8c treatments for Figs. 2E-F: qRT-PCR analysis of

XBP1s mRNA levels in LPS primed human PBMCs treated with PA or a combination of PA and 4μ8c. Statistics as in Fig. 1.

Figure S3. IRE1 regulates lipid-induced CCL2 production in macrophages. (A) qRT-PCR analysis of CCL2 mRNA levels in LPS-primed, PA-stimulated BMDM cells that were treated with STF-083010 or DMSO (control). **(B)** ELISA measurements of secreted CCL2 from the conditioned medium used to culture the cells in A. **(C-D)** qRT-PCR analysis of CCL2 mRNA levels in LPS-primed, PA-stimulated BMDMs that were **(C)** treated with 4μ8c or DMSO (control), or **(D)** transfected with siRNAs against *IRE1α* or *XBP1*. **(E)** ELISA measurements of secreted CCL2 from the cells in D. **(F)** qRT-PCR analysis of CCL2 mRNA levels in LPS-primed, PA-stimulated human PBMCs treated with 4μ8c or DMSO (control). Statistics as in Fig. 1.

Figure. S4 IRE1 perpetuates mtROS production and inflammasome activation. (A) Representative confocal microscopy images of mtROS production in BMDM (in Fig.3A). Mitosox flourence indicator (red) and mitotraker (green) are shown. mtROS (yellow) levels are quantified and depicted in the graph in Fig. 3A. Scale bar: 20μm. **(B-C)** Western blot analysis of caspase-1 activation in LPS-primed, PA-stimulated mouse BMDMs **(B)** treated with STF-083010 or DMSO (control), or **(C)** transfected with siRNAs against IRE1α or XBP1. Pro-caspase-1 (p45) and cleaved caspase-1 (p10) levels are indicated. CE: cell extract. SN: supernatant. Statistics as in Fig. 1.

Figure S5. Treatment of ApoE$^{-/-}$ mice with IRE1α inhibitors suppresses XBP1 mRNA splicing and degradation of canonical RIDD targets. (A) qRT-PCR analysis of XBP1s mRNA levels from spleen tissue of ApoE$^{-/-}$ mice that were fed a Western diet for 12 weeks and treated with STF-083010 or vehicle (Control) for 6 weeks. **(B-C)** qRT-PCR analysis of the mRNA levels of reported RIDD targets in the same tissues as in A. Statistics as in Fig. 1.

Figure S6. Lipid and lipoprotein profiles do not change in animals treated with IRE1 inhibitors. (**A)** Total plasma triglyceride and lipoprotein (VLDL, LDL and HDL) triglyceride levels in STF-083010- and vehicle-treated groups. **(B)** Total plasma cholesterol and lipoprotein (VLDL, LDL and HDL) cholesterol levels in STF-083010- and vehicle-treated groups. **(C-D)** Lipoprotein profiles in control (blue) and STF-083010-treated (red) APOE$^{-/-}$ mice. Statistics as in Fig. 1. (VLDL: very low density lipoprotein; LDL: low density lipoprotein; HDL: high density lipoprotein).

Figure S7. Suppression of *XBP1* mRNA splicing by IRE1 inhibitors *in vivo*. qRT-PCR analysis of XBP1s mRNA levels in spleen of ApoE$^{-/-}$ mice that were fed a Western diet for 12 weeks and treated with 4μ8c or vehicle (control) for 4 weeks. Statistics as in Fig. 1.

Figure S8. IRE1 inhibitors alter plaque composition and inflammation. Immunohistochemical and immunoflourescence analyses of proximal aorta sections obtained from ApoE$^{-/-}$ mice treated with STF-083010 or controls. In each case a representative image is shown on the left and the quantification of the data appears on the right. **(A)** Masson's Trichrome collagen stain (collagen: blue; cytoplasm and muscle fibers: red; n = 5). Scale bar: 200μm **(B)** anti-smooth muscle actin **(**VSMCs marker).Scale bar: 200μm **(C)** anti-CD3 **(**T cell marker). Arrowheads show CD3 positive cells. (n = 5) Scale bar: 50μm. Statistics as in Fig. 1.

Figure S9. IRE1 inhibitors reduce IL-1β levels in tissues and suppress Th1 immune responses. qRT-PCR analysis of IL-1β mRNA levels in **(A)** bone marrow or **(B)** spleen tissue of ApoE$^{-/-}$ mice that were fed a Western diet and were treated with IRE1 inhibitors or vehicle (control). **(C-E)** Flow cytometry analysis of **(C)** IFN-γ, **(D)** IL-4, and **(E)** IL-17 levels in splenocytes activated with PMA/ionomycin (n = 5). Statistics as in Fig. 1.

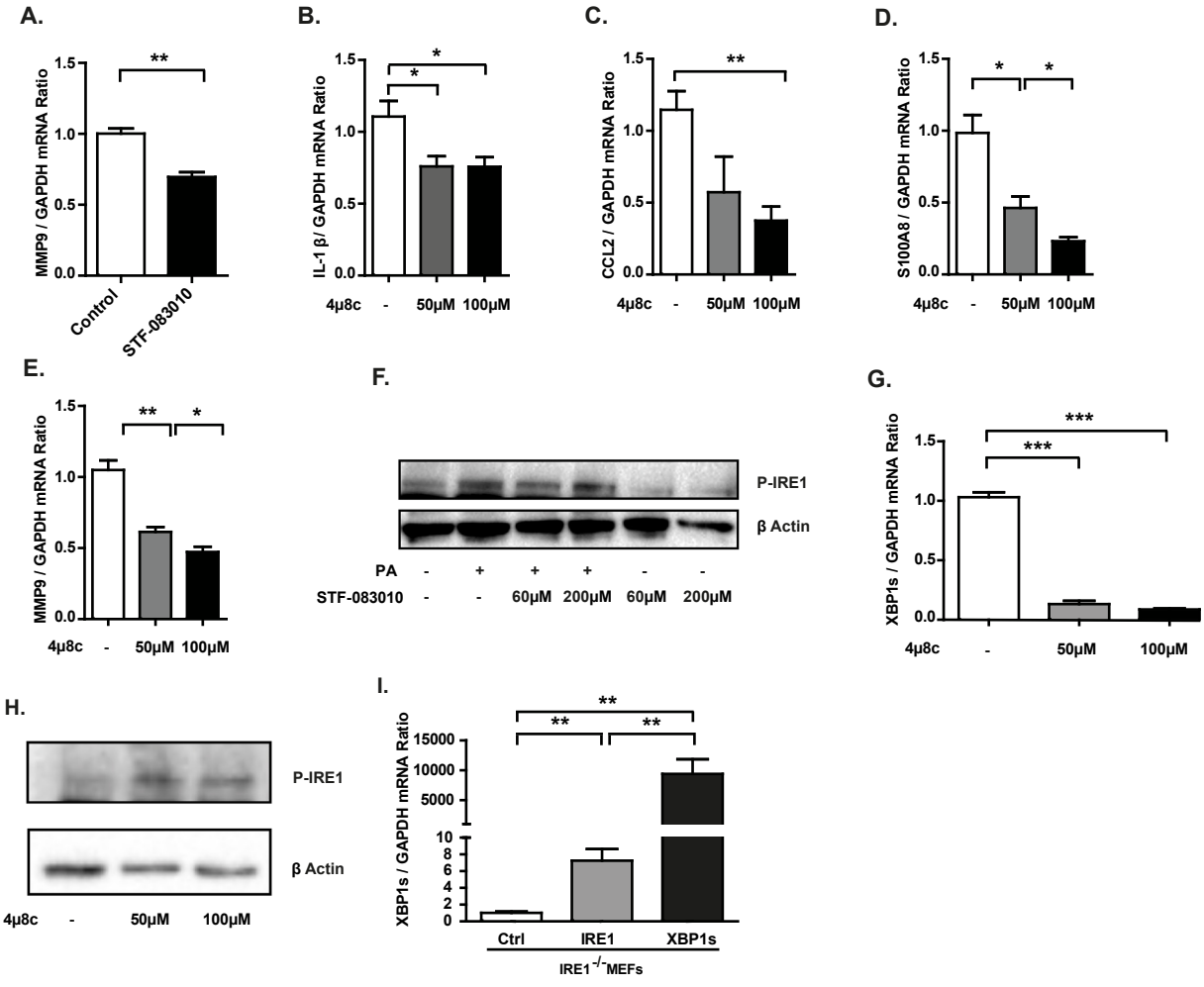
A.
MMP9 / GAPDH mRNA Ratio
1.5
1.0
0.5
0.0
**
Control
STF-083010
B.
IL-1 β/ GAPDH mRNA Ratio
*
*
4μ8c - 50μM 100μM
C.
CCL2 / GAPDH mRNA Ratio
**
4μ8c - 50μM 100μM
D.
S100A8 / GAPDH mRNA Ratio
* *
4μ8c - 50μM 100μM
E.
MMP9 / GAPDH mRNA Ratio
** *
4μ8c - 50μM 100μM
F.
P-IRE1
β Actin
PA - + + + - -
STF-083010 - - 60μM 200μM 60μM 200μM
G.
XBP1s / GAPDH mRNA Ratio
***
***
4μ8c - 50μM 100μM
H.
P-IRE1
β Actin
4μ8c - 50μM 100μM
I.
XBP1s / GAPDH mRNA Ratio
15000
10000
5000
10
8
6
4
2
0
**
**
**
Ctrl
IRE1
XBP1s
IRE1-/-MEFs

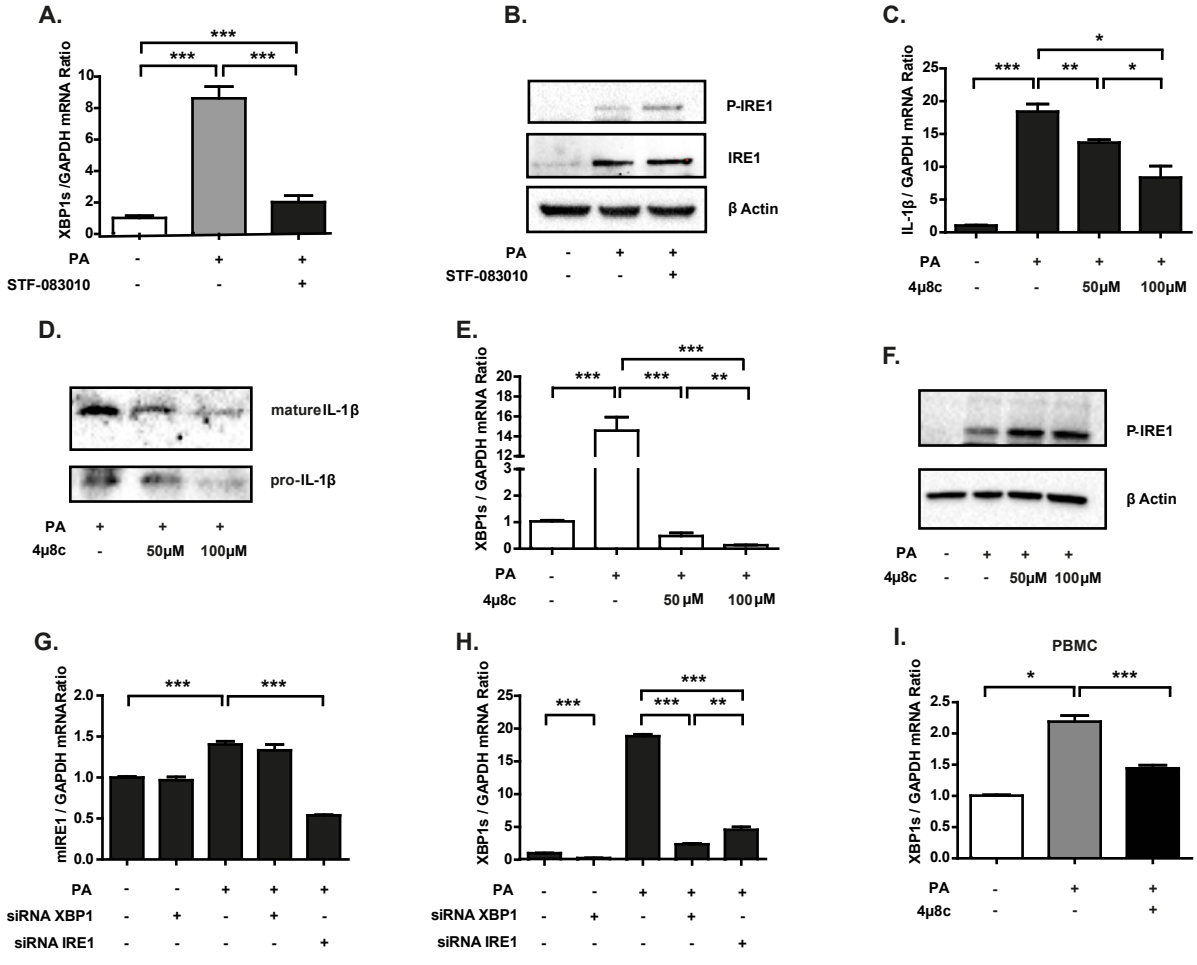
A.
XBP1s /GAPDH mRNA Ratio
***
***
***
PA - + +
STF-083010 - - +
B.
P-IRE1
IRE1
β Actin
PA - + +
STF-083010 - - +
C.
IL-1β / GAPDH mRNA Ratio
***
**
*
*
PA - + + +
4μ8c - - 50μM 100μM
D.
matureIL-1β
pro-IL-1β
PA + + +
4μ8c - 50μM 100μM
E.
XBP1s / GAPDH mRNA Ratio
***
***
***
**
PA - + + +
4μ8c - - 50 μM 100 μM
F.
P-IRE1
β Actin
PA - + + +
4μ8c - - 50μM 100μM
G.
mIRE1 / GAPDH mRNARatio
***
***
PA - - + + +
siRNA XBP1 - + - + -
siRNA IRE1 - - - - +
H.
XBP1s / GAPDH mRNA Ratio
***
***
***
**
PA - - + + +
siRNA XBP1 - + - + -
siRNA IRE1 - - - - +
I.
PBMC
XBP1s / GAPDH mRNA Ratio
*
***
PA - + +
4μ8c - - +

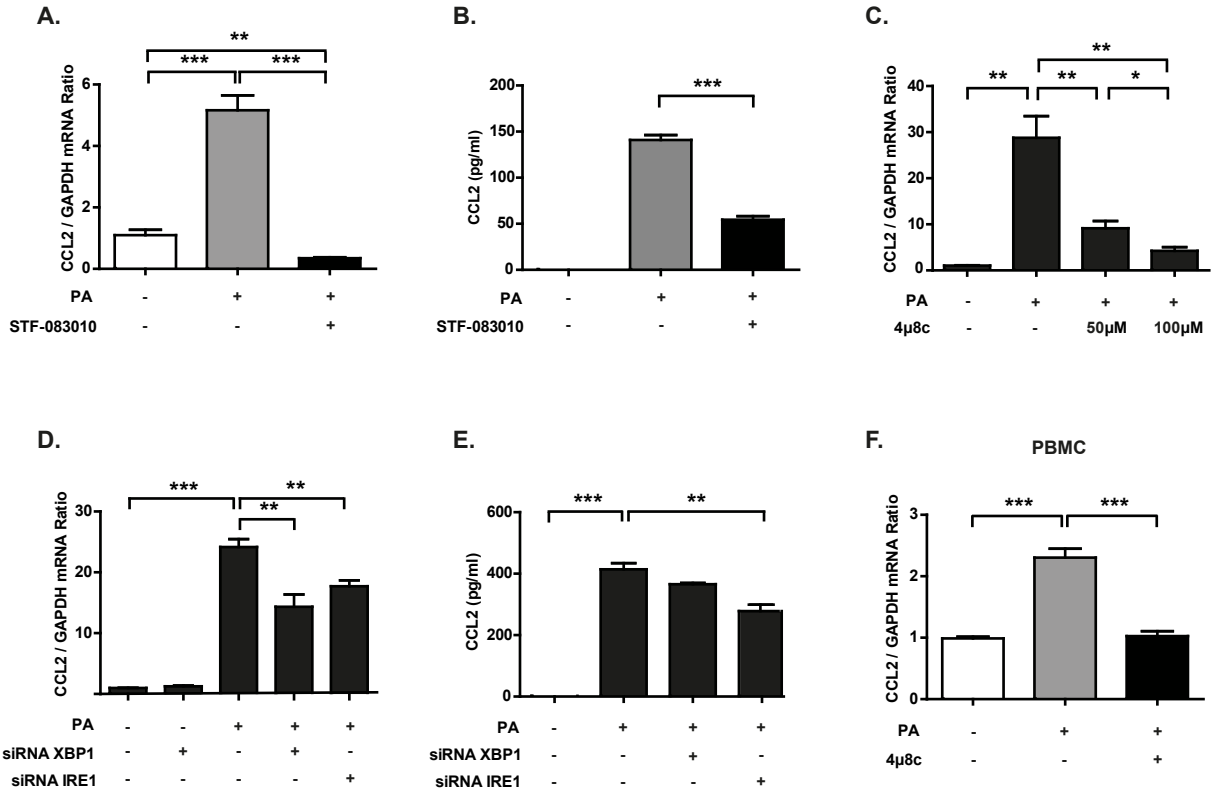
A.
CCL2 / GAPDH mRNA Ratio
PA
STF-083010
B.
CCL2 (pg/ml)
PA
STF-083010
C.
CCL2 / GAPDH mRNA Ratio
PA
4μ8c
50μM
100μM
D.
CCL2 / GAPDH mRNA Ratio
PA
siRNA XBP1
siRNA IRE1
E.
CCL2 (pg/ml)
PA
siRNA XBP1
siRNA IRE1
F.
PBMC
CCL2 / GAPDH mRNA Ratio
PA
4μ8c

A.

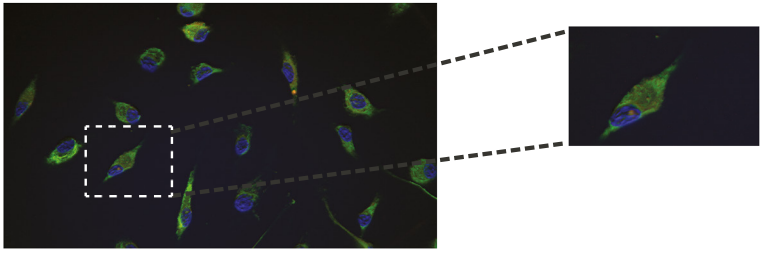

Control

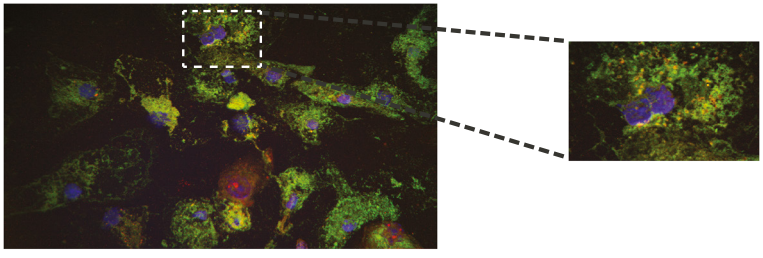

PA

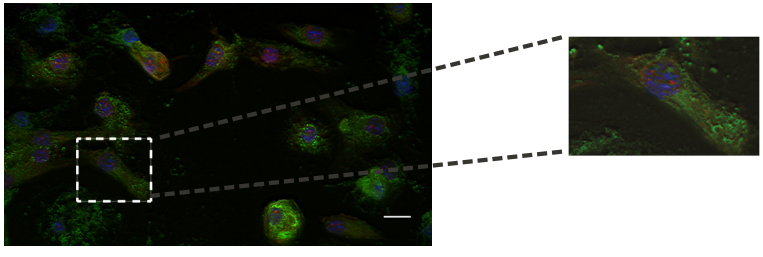

PA + 4μ8C

B.

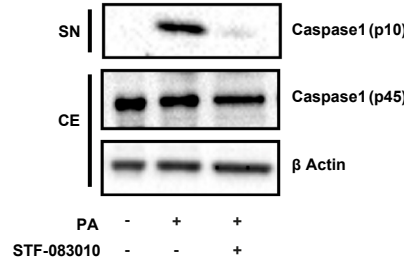

C.

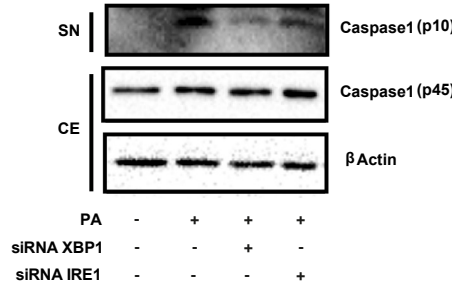

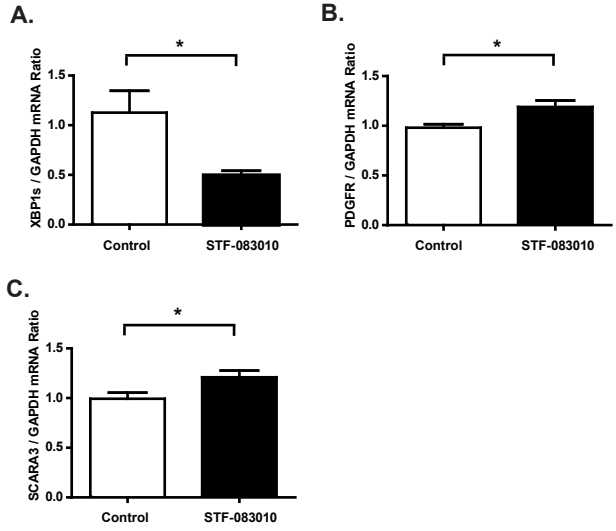
A.
XBP1s / GAPDH mRNA Ratio
1.5
1.0
0.5
0.0
*
Control
STF-083010
B.
PDGFR / GAPDH mRNA Ratio
1.5
1.0
0.5
0.0
*
Control
STF-083010
C.
SCARA3 / GAPDH mRNA Ratio
1.5
1.0
0.5
0.0
*
Control
STF-083010

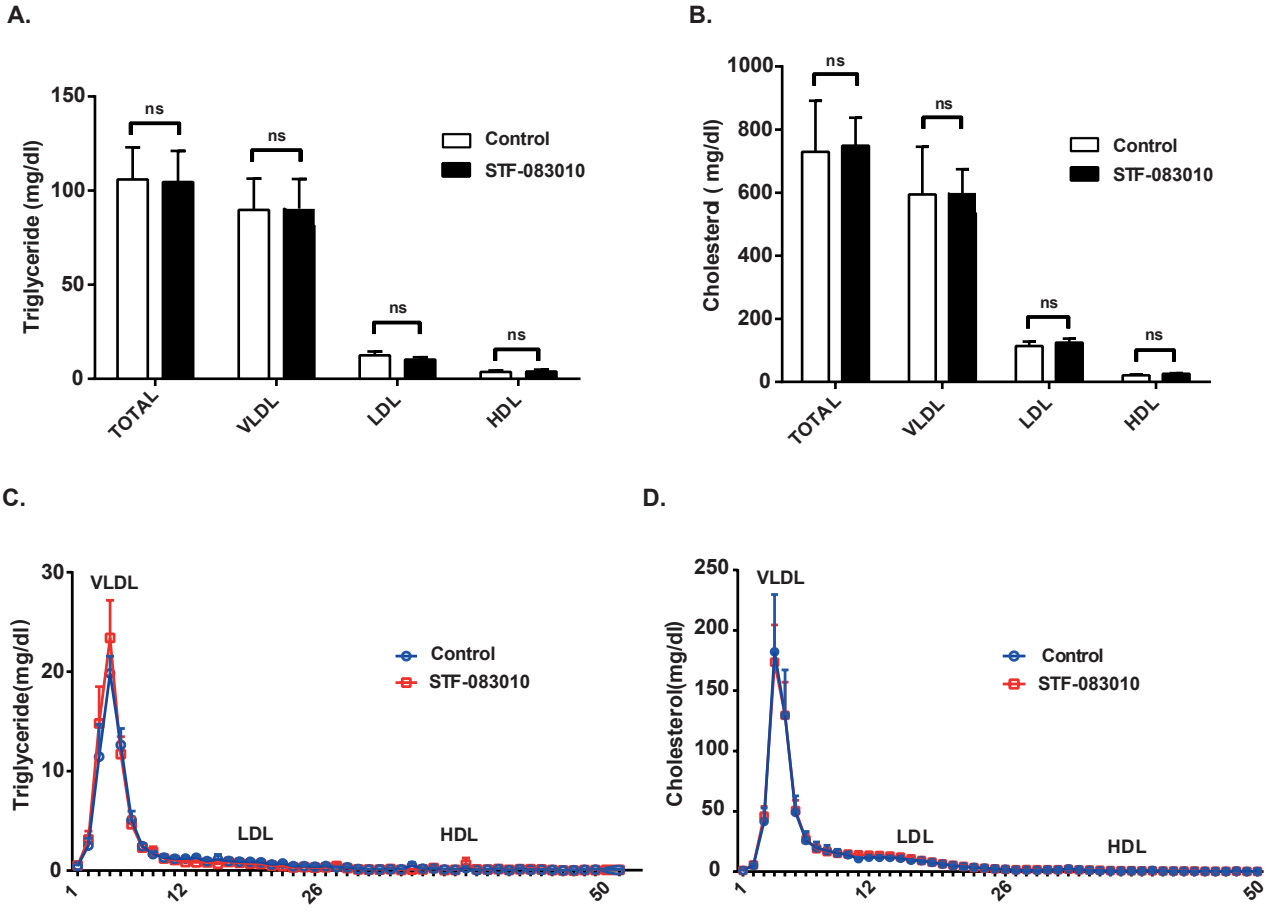
A.
Triglyceride (mg/dl)
150
100
50
0
ns
ns
ns
ns
Control
STF-083010
TOTAL
VLDL
LDL
HDL
B.
Cholesterd (mg/dl)
1000
800
600
400
200
0
ns
ns
ns
ns
Control
STF-083010
TOTAL
VLDL
LDL
HDL
C.
Triglyceride(mg/dl)
30
20
10
0
VLDL
LDL
HDL
Control
STF-083010
1
12
26
50
D.
Cholesterol(mg/dl)
250
200
150
100
50
0
VLDL
LDL
HDL
Control
STF-083010
1
12
26
50

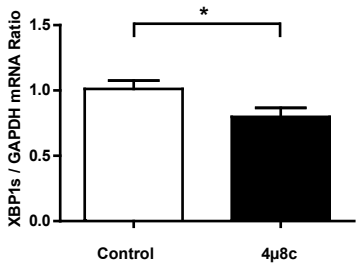
*
XBP1s / GAPDH mRNA Ratio
1.5
1.0
0.5
0.0
Control
4μ8c

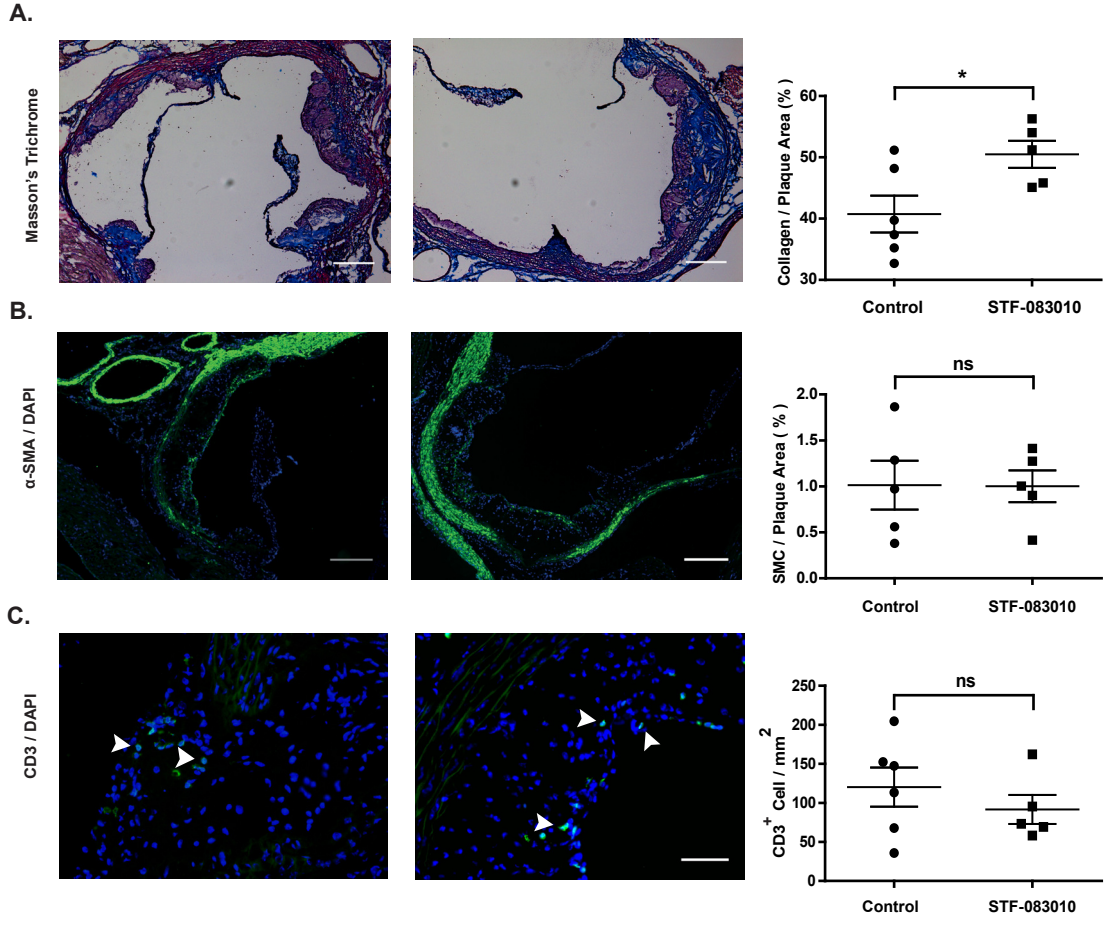
A.
Masson's Trichrome
Collagen / Plaque Area (%)
60
50
40
30
*
Control
STF-083010
B.
α-SMA / DAPI
SMC / Plaque Area (%)
2.0
1.5
1.0
0.5
0.0
ns
Control
STF-083010
C.
CD3 / DAPI
CD3+ Cell / mm2
250
200
150
100
50
0
ns
Control
STF-083010

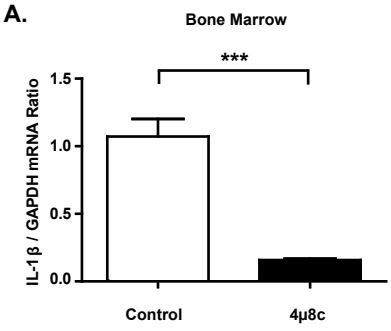
A.
Bone Marrow
***
IL-1β / GAPDH mRNA Ratio
1.5
1.0
0.5
0.0
Control
4μ8c

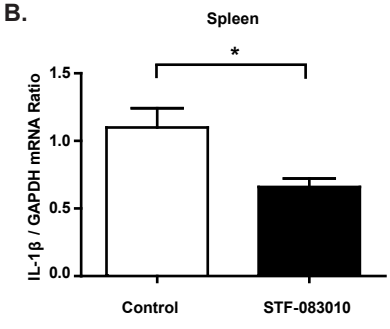
B.
Spleen
*
IL-1β / GAPDH mRNA Ratio
1.5
1.0
0.5
0.0
Control
STF-083010

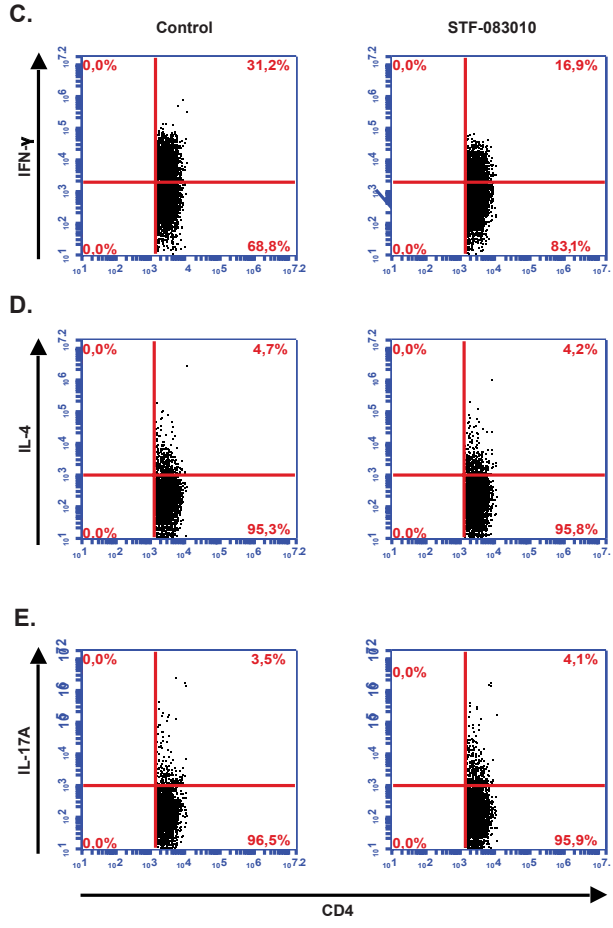
C.
Control
STF-083010
IFN-γ
0,0%
31,2%
0,0%
68,8%
0,0%
16,9%
0,0%
83,1%
D.
IL-4
0,0%
4,7%
0,0%
95,3%
0,0%
4,2%
0,0%
95,8%
E.
IL-17A
0,0%
3,5%
0,0%
96,5%
0,0%
4,1%
0,0%
95,9%
CD4

S. Table 1. Upregulated genes by IRE1α's RNAse domain inhibition (> 1.5-fold change, p<0.05)

Gene	Description	Fold change	p-Value
Gem	GTP binding protein (gene overexpressed in skeletal muscle)	5.28278	0.0197
Aqp9	aquaporin 9	4.26347	5.00E-05
Slc7a11	solute carrier family 7 (cationic amino acid transporter, y+ system), member 11	4.24918	5.00E-05
Chac1	ChaC, cation transport regulator-like 1	4.19526	5.00E-05
Trib3	tribbles homolog 3	4.13576	5.00E-05
Dclk1	doublecortin-like kinase 1	4.10127	0.0061
Slc1a4	solute carrier family 1 (glutamate/neutral amino acid transporter), member 4	3.95788	5.00E-05
Stx1a	syntaxin 1A (brain)	3.95533	0.03755
Soat2	sterol O-acyltransferase 2	3.45083	5.00E-05
Ifrd1	interferon-related developmental regulator 1	3.39259	5.00E-05
Trim46	tripartite motif-containing 46	3.36948	0.00455
Dnmt3l	similar to DNA cytosine-5 methyltransferase 3-like protein	3.32889	0.00085
Zfp827	zinc finger protein 827	3.31926	0.0057
Bcar1	breast cancer anti-estrogen resistance 1	3.24321	0.01765
Fzd4	frizzled homolog 4 (Drosophila)	3.23602	0.04035
Tmeff1	transmembrane protein with EGF-like and two follistatin-like domains 1	3.21715	5.00E-05
Slc7a5	similar to solute carrier family 7	3.17413	5.00E-05
Efcab5	EF-hand calcium binding domain 5	3.15013	0.03165
Gm13889	predicted gene 13889	3.09609	0.02935
Matn2	matrilin 2	3.05605	5.00E-05
Aplp1	amyloid beta (A4) precursor-like protein 1	2.97531	0.0086
Asns	asparagine synthetase	2.95982	5.00E-05
Ddit3	DNA-damage inducible transcript 3	2.94324	5.00E-05
Riiad1	Regulatory Subunit Of Type II PKA R-Subunit (RIIa) Domain Containing 1	2.92652	0.04555
Map6	Microtubule-Associated Protein 6	2.85911	0.0004

S. Table 2. Downregulated genes by IRE1α's RNAse domain inhibition (< 1.5-fold change, p<0.05)

Gene	Description	Fold change	p-Value
Plxnb3	plexin B3	-4.44764	0.03955
Smpd3	sphingomyelin phosphodiesterase 3, neutral	-3.94316	0.006
S100a8	**S100 calcium binding protein A8 (calgranulin A)**	**-3.82977**	**5.00E-05**
Fpr2	formyl peptide receptor 2	-3.76381	0.0461
S100a9	S100 calcium binding protein A9 (calgranulin B)	-3.72286	5.00E-05
Cd177	CD177 antigen	-3.65563	0.04935
Cx3cr1	chemokine (C-X3-C) receptor 1	-3.47787	5.00E-05
Chil3	chitinase-like 3	-3.45585	5.00E-05
Rhobtb1	Rho-related BTB domain containing 1	-3.44936	0.00245
Hpgd	hydroxyprostaglandin dehydrogenase 15 (NAD)	-3.27722	5.00E-05
Syne1	synaptic nuclear envelope 1	-3.08616	0.03485
Gpr34	G protein-coupled receptor 34	-2.98719	0.0171
Ccr2	chemokine (C-C motif) receptor 2	-2.98566	5.00E-05
Sult1a1	sulfotransferase family 1A, phenol-preferring, member 1	-2.87828	0.00875
Ltf	lactotransferrin	-2.83511	5.00E-05
Gm5086	predicted gene 5086	-2.82563	0.00595
Ccl2	**chemokine (C-C motif) ligand 2**	**-2.73314**	**0.006**
Cd69	CD69 antigen	-2.63158	0.0091
Idi1	isopentenyl-diphosphate delta isomerase	-2.60711	0.02395
Ms4a6b	membrane-spanning 4-domains, subfamily A, member 6B	-2.60444	5.00E-05
Il1b	**interleukin 1 beta**	**-2.58506**	**0.0409**
Ccnd1	cyclin D1	-2.57725	5.00E-05
Sesn1	sestrin 1	-2.57127	5.00E-05
Rab3il1	RAB3A interacting protein (rabin3)-like 1	-2.56647	5.00E-05
Gm1966	GTPase, very large interferon inducible 1	-2.56539	0.0001

S.Table 3. Physical and biochemical characterization of ApoE $^{-/-}$ mice treated with STF-083010 and control groups

Variables	Treatment	Control	STF -083010
n		6	6
Body weight (g)	Before	30.3 ± 3.5	28.3 ± 2.2
	After	33.3 ± 5.1	29.8 ± 2.5
Glucose (mg/dl)	Before	120.5 ± 18.5	134 ± 13.3
	After	79.0 ± 11.8	72.6 ± 15.1

S.Table 4. Physical and biochemical characterization of ApoE $^{-/-}$ mice in 4μ8c treated and control groups.

Variables	Treatment	Control	4μ8c
n		7	9
Body weight (g)	Before	28.8 ± 2.7	26.6 ± 1.9
	After	31.1 ± 2.5	28.6 ± 1.2
Glucose (mg/dl)	Before	93.9 ± 30.8	79.2 ± 19.6
	After	91.3 ± 17.0	91.9 ± 20.0